Test of the NILU fog chamber as experiment reactor for droplet growth

Matthias Karl and Susana López-Aparicio

Norsk institutt for luftforskning
Norwegian Institute for Air Research
NILU

Preface

This report covers the work performed as part of the NILU-internal project "Fog-TEST" and the work is a follow-up of a study on the influence of amines on rainfall prepared in the frame of the project "*Amines, emissions to air: A screening project for environmental effects*". Within task 5 of this project "*Model calculations*", task 5.3 addressed the "*Development of methods for modelling fallout of amines directly for the plume*". Aqueous solutions of amines are used in the postcombustion carbon capture to remove CO_2 from the flue gas of a power plant. Volatilization of amines from the scrubbing solution causes emissions of gaseous amines from the capture plant to the surrounding air. In addition droplets emitted from the plant will contain dissolved amines. In the atmosphere, dissolved amines may enhance the probability that very small water droplets can grow to cloud droplet size and cause rain formation in the plume of the CO_2 capture plant. Rain drops falling from the warm plume cloud contain dissolved amines and might cause effects on buildings, materials and human health in the vicinity of the CO_2 capture plant.

2

Contents

4

Summary

Growth of droplets by water vapour condensation is a very effective mechanism for the initial growth of submicron droplets formed from small particles in air. An important effect of amines is to lower the surface tension of aerosol droplets. Decreased aerosol surface tension can lead to a reduction in the critical supersaturation necessary for cloud droplet activation according to Köhler theory. Earlier equilibrium model calculations for monoethanolamine (MEA) showed that the atmospheric gas phase concentration of MEA will determine the actual amount of activated cloud condensation nuclei (CCN). In the project Fog-TEST, a fog chamber was designed and developed to study the characteristics of fog droplets in a reproducible manner. Fog droplet populations generated from MEA solutions exhibited a bimodal distribution with a major mode at 8-10 µm diameter and a weaker mode between 20 and 30 µm. These larger fog/cloud droplets eventually continue to grow and become collector droplets. The experiments support the hypothesis that addition of MEA promotes the formation of supercritical droplets that can cause rainfall.

In postcombustion carbon capture, aqueous solutions of amines are used for removing carbon dioxide (CO_2) from the flue gas of power plants. Amines in the emission of the absorber unit of a CO_2 capture plant will be partly contained in water droplets generated by the wet scrubber and in fresh liquid droplets that formed after the flue gas leaves the stack. Due to their surface-active properties, dissolved amines will enhance the probability that very small water droplets can grow to cloud droplet size and cause rain formation in the plume of the CO_2 capture plant. Rain drops falling from the plume cloud contain dissolved amines and might cause effects on buildings, materials and human health in the vicinity of the CO_2 capture plant.

As part of the project Fog-TEST, a new fog-chamber was designed and characterized in order to cover the needs for performing the experiments. The current fog-chamber, which modification has been based on the experiments performed and the improvement of its functionality, consists basically of the chamber as container, a humidifier and a constant output atomizer. In addition, droplet sampler was modified and adjusted in the framework of the project. In order to analysed the droplet size, a methodology was developed to study droplets impact prints on coated slides by microscopy and subsequent processing and quantification.

From the results obtained within the project is possible to establish that amines, and in particular monoethanolamine (MEA), have influence in the formation of droplets and its growth to cloud droplet size. Experimental results for sodium chloride (NaCl) and MEA solutions are in qualitative agreement with theoretical predictions from Köhler theory.

6

Test of the NILU fog chamber as experiment reactor for droplet growth

1 Introduction

Aqueous solutions of amines are used for removing carbon dioxide (CO_2) from the flue gas of power plants. In the absorber unit of a CO_2 capture plant, amines help to keep the CO_2 gas dissolved in the gas-scrubbing solution. Amines act as a weak base, and neutralize the acidic compounds (carboxylic acid, CO_2-H_2O) and enables a larger amount of CO_2 to become dissolved in the solution by turning the neutral molecules into the ionic form (i.e., bicarbonate ions, HCO_3^- and carbonate, CO_3^{2-}). During this process a certain fraction of amines escapes from the absorber and is emitted to the atmosphere.

Amines in the emission of the absorber unit will be partly contained in water droplets generated by the wet scrubber and in fresh liquid droplets that formed after the flue gas leaves the stack. Monoethanolamine (MEA) has a very high rate of absorption and is the most studied solvent for the removal of CO_2 from flue gases. Therefore, MEA is selected and employed in the fog chamber experiments described in this report.

Amines, like Monoethanolamine (MEA), are used as surface active agents in other industrial applications. Thus their ability to lower the surface tension of water is well known. The growth of a liquid droplet in the atmosphere strongly depends on the surface tension. The surface tension and the partial water vapour pressure will decide the droplet size. The lower the surface tension, the larger the droplet can get. Growth of small droplets by water vapour condensation is a very effective mechanism for the initial growth of particles from sub micrometre sizes to cloud droplets of 10-20 μm size within a few minutes. Amines dissolved in water droplets, as emitted from CO_2 capture plants, may cause enhanced formation of cloud and rain droplets by lowering the surface tension of the initial droplets (Karl, 2008).

Additionally, wash-out of droplets containing amines or amine salts from the plume cloud can contribute to severe corrosion affecting buildings and materials. Amines are used as corrosion inhibitors that can offer both cathodic protection by increasing pH and making proton reduction less favourable, and anodic protection by producing a passivation layer. However, as for ammonia, it is expected that, amines such as MEA can react with acids to produce alkyl ammonium salts. These salts may have similar atmospheric corrosion effects as inorganic ammonium salts, depending on their solubility and hygroscopic properties. Thus amine salt anions might participate in corrosion reactions and be included in corrosion products.

Fog is often described as a cloud on the ground, i.e. a cloud influenced by the surface. However there are some differences in the droplet distribution and fog typically contain less liquid water than clouds. Fog formation typically occurs in very humid air under sub-saturated or slightly supersaturated conditions with

respect to the saturation vapour pressure of water, i.e. near 100% relative humidity. Visibility is reduced inside fogs and from the outside fogs are gray. Mist is a phenomenon of small droplets suspended in air. It can occur as part of natural weather or volcanic activity, and is common in cold air above warmer water, in exhaled air in the cold, and in a steam room of a sauna. Fog is distinguished from mist only by its optical density, as expressed in the resulting decrease in visibility: Fog reduces visibility to less than 1 km, whereas mist reduces visibility to no less than 1 km but less than 2 km. Fog is distinguished from haze by its higher humidity. Haze does not contain activated droplets larger than the critical size according to *Köhler theory*. However, haze particles may act as condensation nuclei for the subsequent formation of mist droplets. In summary the main characteristics of fog are relative humidity near 100%, obstruction of visibility, physiologically appreciable dampness, gray colour, and most importantly: it contains activated droplets larger than the critical size.

The objective of this study is to explore the potential of the in-house fog chamber of NILU as an instrument for testing the impact of dissolved amines on the physical/chemical characteristics of fog droplets.

Rain drops falling from the plume cloud contain dissolved amines. Amines are corrosive, smelly, and affect human health. Rain drops and fog droplets containing amines might cause effects on buildings, materials and human health in the vicinity of the CO_2 capture plant. Results from these experiments are relevant for simulating fog and rainfall from the plume of a CO_2 capture plant, also because there is a health concern during fog situations in the surroundings of the plant.

Before studies on the effect of dissolved amines on droplet growth can be carried out, it should be ensured that the in-house fog chamber at NILU is suitable for this type of experiments. Thus, the scope of this report is to explore the potential of the NILU fog chamber as an instrument for the simulation and evaluation of droplet activation/growth caused by dissolved amines. The reported pilot study is intended as an initial study and a more comprehensive follow-up project about droplet growth and corrosion effect will be proposed, in case the fog chamber proves to be appropriate for the envisaged experiments.

2 Microphysics of condensation and the formation of fog and rain

2.1 Equilibrium vapour pressure over a curved surface

A key aspect of aqueous aerosols is their curved surface. The equilibrium vapour pressure over a curved surface is always larger than the corresponding vapour pressure over a flat surface. When a curved interface exists between air and water, as in a small droplet, there are fewer molecules immediately adjacent to a molecule of water on the surface than when the surface is flat. Therefore, it is easier for the molecules of a small droplet to escape into the vapour phase and the vapour pressure over the curved surface will be greater.

In equilibrium between liquid phase and vapour, both with infinite extension and a flat interface between the phases, the difference of free enthalpy between the phases must disappear and $\mu_{liquid} - \mu_{vapour} = 0$. Thus the vapour pressure for this situation is equal to the saturation vapour pressure, e_s. The ratio between vapour pressure and the saturation vapour pressure is defined by the *saturation ratio* $S = e/e_s$.

The surface energy associated with a curved surface has an important effect on the equilibrium vapour pressure and the rate of evaporation from droplets. The difference between the equilibrium saturation vapour pressure over a flat surface, e_s, and over a spherical (curved) surface, e_s^c, may be calculated from consideration of the change in surface energy which accompanies decrease of surface area. The energy released by a droplet during a change in radius (dr) - through condensation or evaporation - is given by the surface energy multiplied by the change in area.

The saturation ratio S_{Kelvin}, i.e. the relative increase of the saturation vapour pressure over a droplet with radius r compared to over a flat surface (*curvature effect*) is described by,

$$S_{Kelvin} = \frac{e_s^c}{e_s} = \exp\left(\frac{2 \cdot \sigma_p M_p}{r_i \cdot R \cdot T \cdot \rho_p}\right) \approx 1 + \frac{2 \cdot \sigma_p M_p}{r_i \cdot R \cdot T \cdot \rho_p} \qquad (1)$$

σ_p is the average particle surface tension (g s^{-2}), ρ_p the average density of particles (g cm^{-3}), M_p is the molecular weight of the average particle (g mol^{-1}), r_i is the particle radius in the actual size bin (cm), R the universal gas constant (8.31451×10^7 g cm^2 mol^{-1} K^{-1}) and T is ambient temperature (K).

The original formulation of Eq. (1) has been derived by William Thomson (1870) - he later became Lord Kelvin - who deduced it from observations of the capillary rise of water in small tubes. In the following, Eq. (1) is referred to as the *Kelvin equation*.

Equation (1) shows that the vapour pressure required for condensation on very small droplets may be very large. One consequence is, that very large *supersaturation* - excess of vapour pressure over equilibrium vapour pressure over a flat surface - is required to make initial droplets of pure water grow. This

important relationship between droplet size and required supersaturation is schematically shown in Figure 1.
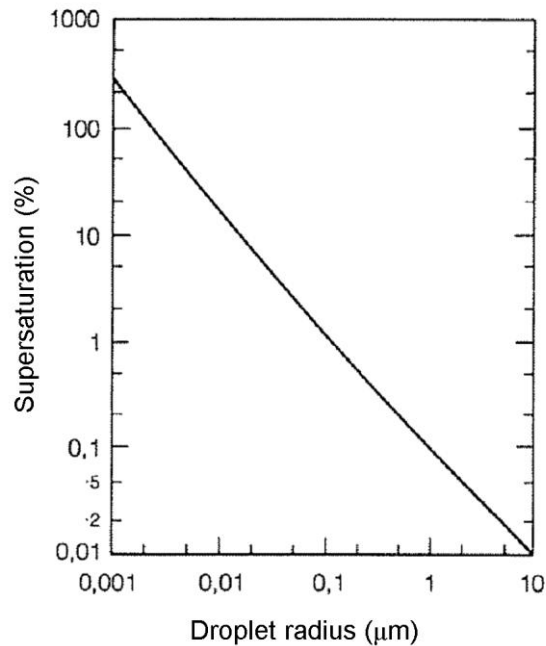
Figure 1:   Supersaturation as function of droplet size (From Roedel, 1992).

Surface tension plays an important role in the curvature effect. Smaller droplets have a tighter curvature. The greater the surface tension of a particle against air, the more likely a water molecule escapes from the surface and the greater the saturation vapour pressure.

2.2   Homogeneous condensation of water

Experiments show that using air which is free of any foreign particles and ions, the saturation ratio must reach about 4-5 or even more in order for droplets to form from the water vapour. In the highly supersaturated air, random collisions of water molecules result in the occasional formation of clusters of molecules, also called droplet *embryos*. When the saturation ratio exceeds the critical value of about 5, the embryos continue to grow by condensation, whereas they would evaporate at a smaller ambient vapour pressure. This process of spontaneous condensation of water molecules is called homogeneous condensation

Supersaturation in the atmosphere seldom exceeds about one percent. Thus it is evident that homogeneous condensation does not occur in the atmosphere. Figure 2 shows the dependency of the saturation ratio required for spontaneous homogeneous condensation on temperature.
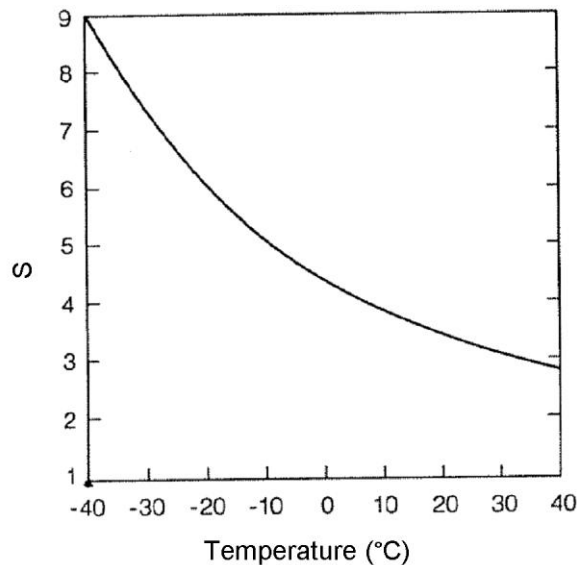
Figure 2:   Relationship between temperature and the supersaturation (S) required for spontaneous homogeneous condensation of water (From Roedel, 1992).

Homogeneous condensation occurs in clean air on negative ions at a saturation ratio of about 4 and on positive ions at a saturation ratio of about 6. Ions in the atmosphere are ubiquitous and are formed by cosmic rays or by radioactive decay products. In the Wilson cloud chamber, homogeneous condensation on ionizing particles is achieved by suddenly expanding the chamber (adiabatic cooling) and hence generating very large supersaturation.

2.3   Heterogeneous condensation

The main conclusion of section 2.1 and the Kelvin equation was that very tiny droplets can only exist in vapour that is supersaturated by several 100%, while somewhat larger droplets can exist at a vapour pressure that is only a few *‰* above the vapour pressure over an infinite flat water surface.

In the atmosphere, numerous small solid and liquid particles exist, on some of which condensation of water molecules can occur without the powerful inhibiting effect of curvature. These foreign particles, also called "nuclei" provide an initial radius for the formation of cloud/fog droplets. According to Figure 1, a wettable particle with a radius of 1 μm can be a condensation nuclei already at a supersaturation of 0.1%. Some of the nuclei are soluble in water (hygroscopic), others are wettable but insoluble, and others are water resistant (hydrophobic).

A second factor that affects the saturation vapour pressure is that of dissolved solutes (dissociated or undissociated), the *solute effect*. When a solute dissolves in solution, the saturation vapour pressure of the solvent is reduced. For a pure non-volatile solute (not evaporating), the vapour pressure is zero. By adding molecules of a solute to the solution, solvent molecules on the droplet surface are replaced by solute molecules. Since the total vapour pressure over the solution is the sum of the vapour pressures of the solvent and the solute, the total vapour pressure over the solution, e_s^h, will be less than over the pure solute, e_s, alone. From

12

Raoult's Law the saturation ratio S_{Raoult} over a dilute liquid water solution is described by:

$$S_{Raoult} = \frac{e_s^h}{e_s} \approx 1 - \frac{3 \cdot m_s \cdot v \cdot M_w}{4\pi \cdot r_i^3 \cdot \rho_w \cdot M_s}$$ (2)

With m_s being the mass of solute in the droplet (g), M_w the molar weight (g mol^{-1}) and ρ_w the density of liquid water (g cm^{-3}). M_s is the molar weight of the solute (g mol^{-1}). The van't Hoff factor v describes the number of moles of ions produced per mole of solute, with $v=2$ for sodium chloride (NaCl) and MEA.

While the curvature effects increases the vapour pressure over small droplets, the solute effect decreases it. The solute effect affects primarily small particles, since small particles have a higher concentration of solute than the larger particles. Equation (2) shows that for a specific mass of dissolved material, the equilibrium vapour pressure over a solution decreases rapidly with decreasing radius of the droplet.

2.4 Growth of fog droplets

Kelvin and Raoult describe competing effects: while the curvature tends to increase the saturation vapour pressure over small water droplets, the solute tends to decrease it. The combination of the Kelvin and Raoult effect results in the *Köhler equation* with the principal approximate formulation (Köhler 1936):

$$S' = \frac{e_s'}{e_s} \cong 1 + \frac{a}{r} - \frac{b}{r^3}$$

with

$$a = \frac{2 \cdot \sigma_p M_p}{R \cdot T \cdot \rho_p} \qquad\qquad b = \frac{3 \cdot m_s \cdot v \cdot M_w}{4\pi \cdot \rho_w \cdot M_s}$$ (3)

The Köhler equation relates the saturation vapour pressure of water over a curved surface containing solute, e_s' to that over a flat surface without solute.

$$S' \cong 1 + \frac{2 \cdot \sigma_p M_p}{r_i \cdot R \cdot T \cdot \rho_p} - \frac{3 \cdot m_s \cdot v \cdot M_w}{4\pi \cdot r_i^3 \cdot \rho_w \cdot M_s}$$ (4)

In Figure 3, the equilibrium saturation ratio, S' (solid curve), is shown for a solution droplet formed on an ammonium sulphate condensation nucleus, together with the curves of S_{Kelvin} (dashed line above $S = 1.00$) and S_{Raoult} (dashed line below $S = 1.00$). Supposed, the ambient saturation ratio is $S = 1.00$ (RH = 100%), or in other words supersaturation is 0%, then a particle with a radius of 0.04 µm will start to grow by adding water molecules, and S' increases along the equilibrium saturation curve (solid line), as long as ambient $S > S'$. At maximum equilibrium saturation ratio, the critical saturation ratio S^* is reached. The corresponding radius is the critical radius r^*. Particles starting with a radius smaller than the critical radius cannot grow further to cloud-drop size unless the

ambient saturation ratio exceeds the critical saturation ratio. Particles with initial sizes larger than the critical radius can activate if $S > S'$ over these droplets. Therefore a droplet starting with a radius 0.1 µm can grow freely into a cloud droplet at 0% super saturation.
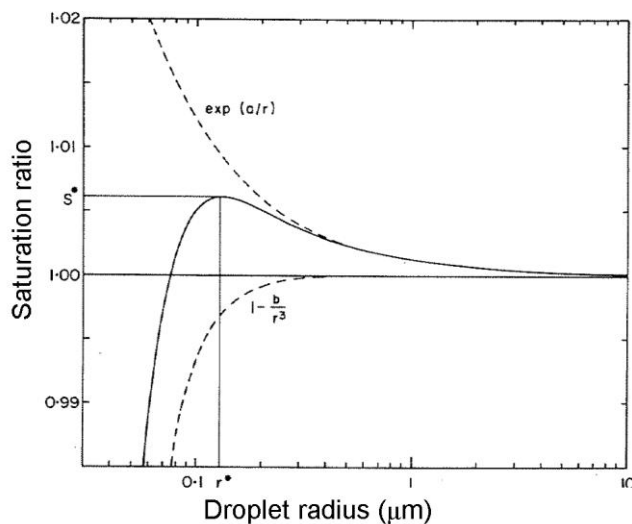
Figure 3:   *Equilibrium saturation ratio of a solution droplet formed on an ammonium sulphate condensation nucleus of mass 10^{-16} g. (From Rogers and Yau, 1989).*

The critical radius, r^*, for growth to cloud droplets and the critical saturation ratio, S^*, can be calculated using:

$$r^* = \sqrt{\frac{3b}{a}} \qquad\qquad S^* = 1 + \sqrt{\frac{4a^3}{27b}}$$

(5)

In Figure 3, two distinct different regimes can be found: droplets of sizes below the critical radius, and droplets with sizes above the critical radius. In a droplet population with droplets of different sizes, larger nuclei deliquesce first, as air becomes saturated. Droplets that have formed on larger nuclei will first pass the maxima of the Köhler curve (critical supersaturation) that corresponds to the critical radius and thus continue to grow freely by condensation. As water vapour molecules continue to condense until equilibrium vapour pressure is reached, those droplets that did not pass the critical supersaturation barrier will shrink due to evaporation to a smaller size, allowing the larger droplets to continue to grow. That means, the droplets that formed on the large nuclei after they passed the barrier will grow further by condensation on cost of the droplets that formed on the smaller nuclei.

Assuming that sufficient condensation nuclei are available in an air parcel and that an appropriate degree of supersaturation is given, a cloud/fog droplet will grow by diffusion of water molecules towards the droplet followed by condensation. The growth of a droplet of mass m_p and radius r is given by the diffusion law:

14

$$\frac{dm_p}{dt} = 4\pi R^2 D \frac{d\rho_v}{dR} \qquad (6)$$

Where D is the diffusion coefficient of water vapour in air, and ρ_v is the vapour density. Integration of Eq. (6) over the radial distance R, from the surface of the droplet at $R = r$ to $R = \infty$, to get:

$$\frac{dm_p}{dt} = 4\pi r D \left(\rho_{v,\infty} - \rho_{v,r} \right) \qquad (7)$$

The vapour densities $\rho_{v,r}$ and $\rho_{v,\infty}$ are the boundary conditions at, and far from, the surface of the droplet. The mass change of a spherical droplet due to condensation can also be expressed as change of radius with time by:

$$\frac{dm_p}{dt} = 4\pi r^2 \frac{dr}{dt} \rho_w \qquad (8)$$

Combining Equation (7) and (8), the rate of growth of the droplet due to diffusion of vapour is:

$$\frac{dr}{dt} = \frac{D}{r} \left(\frac{\rho_{v,\infty} - \rho_{v,r}}{\rho_w} \right) \qquad (9)$$

Eq. (9) is valid for the condition that $\rho_{v,r}$ and hence the temperature of the droplet remains constant with time.
However, during condensation, the droplet will gain heat Q due to the release of latent heat L, at a rate given by:

$$\frac{dQ}{dt} = L \frac{dm_p}{dt} = 4\pi r L D \left(\rho_{v,\infty} - \rho_{v,r} \right) \qquad (10)$$

There is also heat loss due to the thermal conductivity of air, λ. The heat flow through the surface of the droplet of radius r and its surroundings at distance R is:

$$\frac{dQ}{dt} = 4\pi r^2 \lambda \frac{dT}{dR} \qquad (11)$$

Again integrating from $R = r$ to $R = \infty$, one obtains:

$$\frac{dQ}{dt} = 4\pi r \lambda \left(T_\infty - T_r \right) \qquad (12)$$

Combining Equation (10) and (12) for dQ/dt, it can be shown that the droplet is warmer than its surrounding by the amount:

$$\left(T_\infty - T_r \right) = \frac{L D \left(\rho_{v,r} - \rho_{v,\infty} \right)}{\lambda} \qquad (13)$$

Equation (9) and (13) can be solved, using the Clausius-Clapeyron and Köhler expressions, to obtain the growth rate of a droplet under a given set of conditions. Table 1 presents some typical results for the growth history of a droplet.

Table 1: *The growth history of a droplet with initial radius of 0.75 μm, containing 10^{-14} g of NaCl at an atmospheric level where relative humidity is 100.05%, pressure is 900 mbar, and $T = 273$ K (from Mason, 1971).*

Radius (μm)	Time
0.75	0
1.0	24 s
2.0	130 s
4.0	1000 s
10	2700 s
20	2.4 hr
30	4.9 hr
50	12.4 hr

Growth of droplets by water vapour condensation is a very effective mechanism for the initial growth of aerosol particles from sub micrometre sizes to 10-20 μm sizes which all occurs within minutes. However the further growth of a droplet is a slow process. For instance, a droplet with initial radius of 0.75 μm needs about 12 hours under constant atmospheric super saturation of 0.05% to grow to 50 μm by the process of condensation (Table 1).

In a fog/cloud droplet distribution with 10 μm and larger sized droplets, the larger drops will start to fall and collect smaller droplets. Larger droplets will collide with the smaller ones and grow further by *coalescence*. Whereas growth by condensation tends to slow down as the droplet becomes larger, the larger droplets formed by coalescence grow even faster, as can be seen in Figure 4. Large droplets fall faster than smaller droplets, overtaking and capturing of the smaller ones that lie in their falling path. A large droplet will only collide with a fraction of the smaller droplets, because some are swept aside in the airstream around the large droplet.
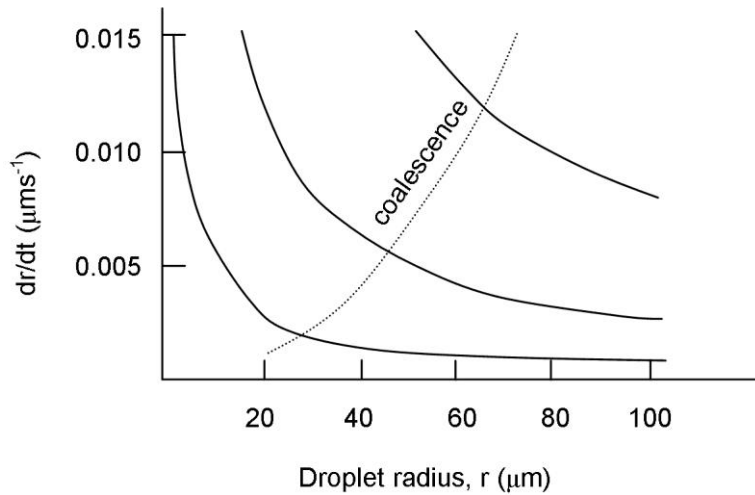
Figure 4   Examples of the rate of growth of cloud droplets in a cloud with fixed liquid water content of 1 g cm^{-3} by coalescence (dashed line) and by condensation (solid lines), assuming increasingly supersaturated water vapour pressures (shown in mbar above the saturation value) in the air surrounding the droplet. (From Taylor, 2005).

The collection efficiency describes the probability by which two particles collide and stick together to form a new and larger drop (coalesce). The growth of a falling drop of mass m as a result of the collision/coalescence can be described by,

$$\frac{dm}{dt} = \pi \cdot E \cdot \left(V_{t,c} - V_{t,d}\right) \cdot \left(r_c + r_d\right)^2 \cdot L \qquad (14)$$

E is the collection efficiency, L is the liquid water content (g) of the small drops, V_t is the terminal fall speed (cm s^{-1}) of the collector drop (index c) and the smaller drops (index d), r_c is the radius of the collector drop (cm) and r_d the radius of the smaller drops. For the terminal fall speed the following approximations can be made, depending on the given size range of the falling drop:

Terminal fall speed		*Size range*
$V_t = k_1 \cdot r^2$	$k_1 = 1.19 \cdot 10^6 \, cm^{-1} s^{-1}$	Up to 30 μm
$V_t = k_2 \cdot r$	$k_2 = 8 \cdot 10^3 \, s^{-1}$	30 μm to 0.6 mm
$V_t = k_3 \cdot \sqrt{r}$	$k_3 = 2.01 \cdot 10^3 \, cm^{-1/2} s^{-1}$	0.6 to 2 mm

$$(15)$$

The terminal velocity of droplets with size below 30 μm follows the Law of Stokes, and increases proportional to r^2. A droplet of $r=10$ μm for example has a terminal velocity of 1.2 cm s^{-1} while a droplet $r=30$ μm has a terminal velocity of 11 cm s^{-1}. It should be noted that a droplet of the size of 10 μm can only travel a distance of a millimetre in air with 90% relative humidity, before it evaporates. Gravitational collection is the most important mechanism by which clouds form rain drops in warm clouds (clouds with temperatures above 0°C). Droplet collection efficiencies for different sizes of collector drops and the captured droplets are presented in Table 2.

Table 2:   *The droplet collection efficiency as function of radius R of the collector drop and radius r of the collected droplet.*

Radius	R=					
r=	10 μm	20 μm	50 μm	100 μm	250 μm	500 μm
5 μm	0.04	0.05	0.19	0.48	0.57	0.56
10 μm	–	0.17	0.53	0.70	0.67	0.61
20 μm	–	–	0.58	0.65	0.57	0.48
30 μm	–	–	0.58	0.51	0.49	0.49

2.5   Microstructure of ambient fogs

The most studied and therefore well-described fog types are those associated with *radiative cooling* over land. These can be divided among:

1) radiation fog,
2) high-inversion fog, and
3) advection fog.

Radiation fog usually forms near the surface under clear skies in stagnant air in association with an anticyclone. The main mechanism is radiative cooling, but the opposing influences of upward soil heat flux, as well as warming effects and moisture losses through dew deposition from turbulent mixing in the stable boundary layer largely determine the likelihood and timing of radiation fog formation (Gultepe et al., 2007, and references therein). High-inversion fog usually forms in valleys within a deep moist layer capped by a strong inversion (Holets and Swanson, 1981). Another relatively well-studied fog type is associated with the advection of a moist air mass with contrasting temperature properties with respect to the underlying surface and is therefore referred to as advection fog.
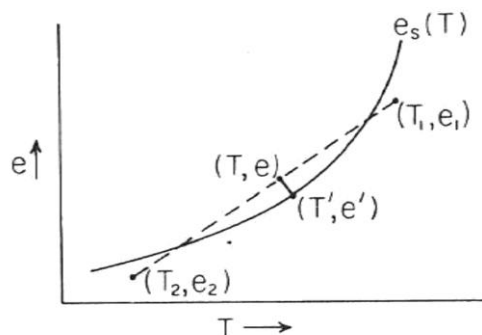
Figure 5   Hygrometric chart showing the isobaric mixing of two air samples.

Isobaric mixing of two (non-saturated) air masses can also explain fog formation, because the possibility exists that the mixture is super saturated. In this event condensation occurs and a fog forms in the mixture. The isobaric condensation process can be described using a hygrometric chart (Figure X). The slope de/dT describes the isobaric condensation. The intersection of this line with the saturation vapour pressure curve $e_s(T)$ defines a point with coordinates T',e', which corresponds of the mixture of air masses after condensation has occurred.

Fog formation typically occurs in aerosol-laden surface air under high relative humidity conditions, ranging from *sub-saturated to slightly supersaturated conditions* (Pruppacher and Klett, 1997). Processes shaping the microstructure of fog include:

- droplet activation,
- diffusion growth of droplets,
- droplet growth related to radiative cooling,
- turbulent mixing,
- differential gravitational settling of drops of different size.

Observations by Houghton and Radford (1938) and later by other researchers showed that fogs, unlike clouds, are characterized by relatively low water contents (generally less than 0.2 g m^{-3}), small drops (typically between 2.5 μm and a few tens of micrometers, with a typical diameter between 10 and 20 μm), small number concentrations (1 to few hundred per cubic centimetre), and liquid water contents ranging between 0.05 and 0.5 g m^{-3}.
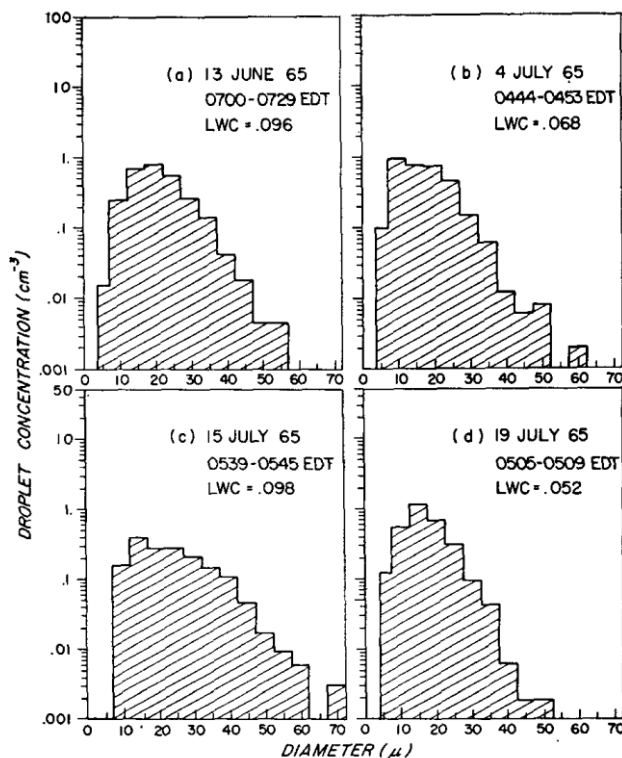
Figure 6:   Histograms of the mean droplet size distribution, measured by a hologram camera, taken during four different fog cases (adopted from

Kunkel, 1971). The hologram camera was installed and operated at Otis AFB, Falmouth, Massachusetts.

According to Kunkel (1982), one may distinguish among three stages during a fog event. In the *formative stage*, the droplet number concentration increases with time resulting in increasing liquid water content, *LWC*, while the mean drop size may remain the same or may increase slightly. During the *mature stage*, the number concentration, *LWC*, and mean drop size fluctuate rather strongly around generally constant values. The final *dissipative stage* is a period of decreasing drop concentration, drop size, and *LWC*.

Figure 6 shows the droplet size distributions from four different fog events measured by a hologram camera (Kunkel, 1971). In a recent study, Okuda et al. (2009) report on a direct photographic method to measure the droplet size distribution inside fogs. The instrument consists of a digital camera and a stroboscope with a diffuser and was mounted on a tethered hot air balloon to measure directly in the fog at different heights. Figure 6 shows a vertical profile of the droplet concentration during a fog observed with the photographic method attached to the hot air balloon. The visibility during the observed fog was less than 500 m at the surface.
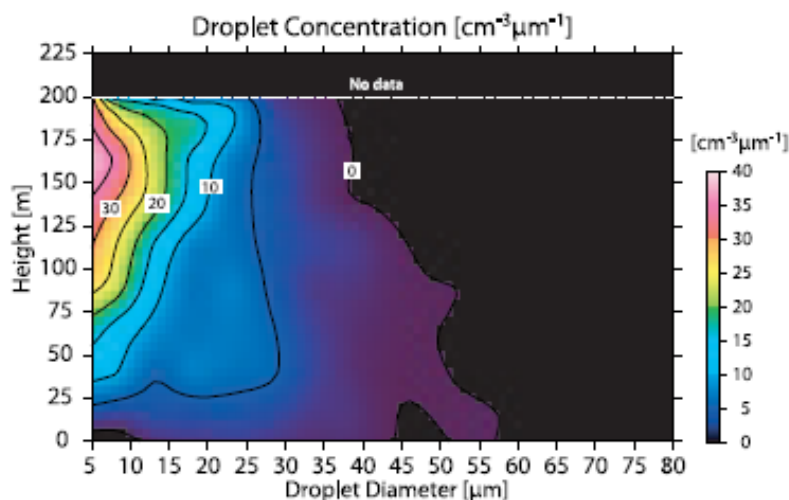
Figure 7: Vertical profile of droplet (number) concentrations (in cm^{-3} μm^{-1}) on 10 July 2006 in a fog observed in Northwest Japan (adopted from Okuda et al., 2009). The contour interval is 5 cm^{-3} μm^{-1}. The fog top was near 200 m height. The balloon could not rise above 200 m because of strong winds above the fog layer.

Fog droplets scavenge soluble gases like nitric acid, ammonia, or amines, and act as a medium for various aqueous phase reactions, including the oxidation of absorbed SO_2 to sulphate (Pandis et al., 1990). The formed sulphate is non-volatile and will increase the dry mass of the particulate phase after the cloud/fog has evaporated. Fog droplet number concentration strongly depends on the phase and chemical composition of particles that serve as the nuclei. It is also largely

determined by how many aerosol particles are activated as nuclei. Aerosol activation depends on aerosol number concentration, mean radius and standard deviation of aerosol size distribution, and aerosol solubility. Droplets, unlike dust particles, are unstable. Any contact with a solid surface or another droplet makes the droplet disappear as an entity. Therefore, unlike dust particles for example, droplets cannot be collected on a filter paper for subsequent physicochemical analysis in the laboratory. Also it is difficult to collect cloud as individual droplets because a single cloud droplet has a tiny volume.

2.6 Effects of surfactants on droplet activation and growth

Water has a relatively high surface tension, because of strong hydrogen bonds. Surface-active compounds (*surfactants*) substantially lower the surface tension of water droplets. There is considerable experimental evidence that organics in aerosols can lower surface tension of droplets in comparison to pure water droplets (Shulman et al., 1996, Tuckermann and Cammenga, 2004). It is also known that amines currently used in CO_2 capture, like MEA, lower the surface tension of water droplets (Vázquez et al., 1997; Águila-Hernández et al., 2001; Águila-Hernández et al., 2007).

By lowering the surface tension, the activation barrier for the growth of small droplets into cloud droplets is lowered (Hitzenberger et al., 2002). Surface-active compounds may have a significant potential to increase cloud droplet number concentration and thus radiative forcing of clouds (Nenes et al., 2002; McFiggans et al., 2006). Facchini et al. (1999) reported that measured cloud water samples taken in the Po Valley (Italy) containing high fractions of organic surfactants, showed a decrease in surface tension by up to one-third relative to pure water. They estimate that a 30% decrease of the surface tension results in a 20% increase of cloud droplet number concentration.

Tiny water droplets that contain dissolved amine can grow larger and can exceed the critical radius. Aerosol particles then grow into cloud droplets at certain levels of humidity, this process is known as *activation*. These particles will act as *cloud condensation nuclei* (CCN). There will always be sufficient small pre-existing particles on which initial cloud droplets can form. However, adding amines to small water droplets will lower their surface tension and in consequence allow for growth out of the equilibrium state at lower supersaturation. Thus amines enhance the probability that very small water droplets can grow to cloud droplet size (10-20 μm) and cause cloud formation in the plume of the CO_2 capture plant. Because of the reduction in the surface tension that counteracts the Kelvin effect, initial droplets can pass the critical barrier and continue to grow by condensation and become larger droplets that can form fog/cloud droplets. Finally, the larger droplets of the initial droplet distribution grow further by condensation and coalescence and eventually reach the size of rain drops. If the falling rain drops become large enough (about 300 μm), they will be able to reach the ground.

While a reduction in surface tension of water droplets alone will always lead to a reduction of the critical supersaturation and increase number of activated droplets, it is unclear if this will be the dominating effect under atmospheric conditions. For example, the formation of insoluble organic films on the surface of droplets might change the critical supersaturation (Sorjamaa et al., 2004). Li et al. (1998) studied

the effect of surfactant partitioning between the bulk solution of the droplet and the surface layer of the droplet on surface tension. For the mixture of sodium dodecyl sulphate (SDS) and sodium chloride (NaCl) they found an increase in critical supersaturation, compared to the case when surfactant partitioning is not taken into account. The effect of surfactant partitioning is two-fold: first, it affects the surface tension (Kelvin effect) and second, it affects the Raoult effect by decreasing the number of moles of solute in the droplet since the soluble surfactant displaces the NaCl. Hence the high molecular weight soluble surfactant inhibits activation of NaCl nuclei into droplets.

Furthermore, organic compounds that do not readily dissolve in water, such as slightly soluble compounds (e.g. difunctional carboxylic acids), will only become gradually dissolved in the growing droplet and thus affect the shape of the Köhler curve (Shulman et al., 1996). Although the effect of dissolution kinetics is not sufficient to inhibit CCN activation, affected droplets under certain conditions may experience slower growth and require a higher level of supersaturation to activate (Asa-Awuku and Nenes, 2007).

The simplest picture of the organic film structure is that of a film formed by long-chain saturated fatty acids and alcohols. The OH or COOH group is attracted by water and dips into it, but is unable to pull the adjacent hydrocarbon chain with it, thus leaving it standing vertically (see Figure 8). Molecules whose hydrophobic groups (e.g. their hydrocarbon chain) have less than four or five carbon atoms are generally water-soluble; they may alter the surface properties (lowering surface tension) of water but by themselves will not form films. In this respect, a short-chained amine like MEA will most likely not form a film on the droplet surface, while other amines with a longer carbon chain, like N-tert-butylethanolamine (CAS no. 4620-70-6), are probably subject to organic film formation.
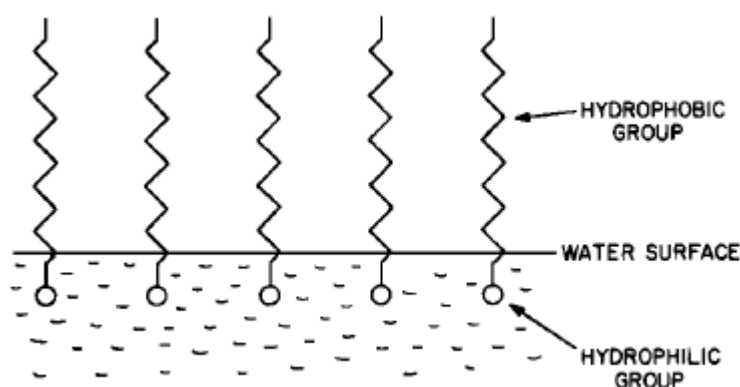
Figure 8: *The orientation of surface-active organic molecules at the water surface. Schematic picture of the organic film formed on a droplet (Adopted from Gill et al., 1983).*

In their review of organic films on aerosol particles, Gill et al (1983) concluded that organic films are probably common on atmospheric aerosol particles and that they may occur under certain circumstances on fog droplets, cloud droplets, and snowflakes. An important early finding by Langmuir and Langmuir (1927) was,

that a monolayer (one complete molecular layer) film of oleic acid lowered the rate of evaporation of ether from water solution significantly. The presence of organic films will increase the lifetimes of aerosol particles, fog droplets, and cloud droplets, both by inhibiting water vapour evaporation and by reducing the efficiency with which these atmospheric components are scavenged by larger hydrometeors (e.g. McDonald, 1963). The transport of gaseous molecules into and out of the aqueous solution of the droplet will be impeded by factors of several hundred or more when organic films are present (Gill et al., 1983).

Based on a simple implementation of Köhler theory and a simplified parameterization of the surface tension of droplets containing amines, Karl (2008) suggested that the concentration of dissolved amine will determine the number of small water droplets that become activated into CCN. For a given population of accumulation mode particles and a gas phase concentration of 0.1 ppbv MEA, the size threshold for the activation (activation diameter) was calculated to be 0.2 µm (at a supersaturation of 0.1%). The activation diameter was reduced to 0.14 µm when the MEA gas phase concentration was increased to 1 ppbv, and at the same time, the number concentration of CCN increased from 600 cm^{-3} to 1380 cm^{-3}. It is noted that the effects of surfactant partitioning and dissolution kinetics were not taken into account in that work. MEA was used as a model amine compound by Karl (2008) and thus it can be justified to omit the discussed effects, since 1) MEA is highly soluble in water and readily dissolves, and 2) MEA is a short-chained amine (two carbon atoms).

3   Characterization of the NILU fog chamber

The fog chamber in the corrosion laboratory is a useful instrument to simulate conditions of fog from the industrial wet scrubbing process. The original design of the fog chamber was modified in the project and currently consists basically of the chamber, an humidifier and an atomizer, components which will are described below.

Wet scrubbers are applied in the absorption unit of CO_2 capture facilities that are used for the absorption and removal of CO_2 from the flue gas of power plants. In the absorber, humidity is well above 100% relative humidity and temperature is about 55°C. The wet scrubber emits a wide spectrum of fine water droplets from several 100 nm to several µm sizes and gaseous compounds, like the amines used for the absorption of CO_2.

3.1   Geometry of the chamber

The fog chamber consists of three parts: two cylinders and a cone on top (Figure 9) made of polycarbonate. The two cylinders have a diameter of 96 cm, the lower one is 65.5 cm high and the upper one is 50.5 cm high. The cone has an approximate height of 39.5 cm. The total volume of the chamber is 0.94 m^3. The build-up of the chamber from the three construction elements requires two persons.

We recommend to install a pulley tackle to lift the upper cylinder, which is the heaviest part of the construction. This would allow one person to build up the chamber without assistance.

3.2 Operation principle and setup

The design of the fog chamber was performed during the project according to the experimental needs (Figure 9). A humidifier is connected under the chamber to the main inlet (Figure 9) to provide the required high humidity conditions for the experiments in addition to hot steam.

A constant output atomizer Model 3076 from TSI (http://www.tsi.com/en-1033/index.aspx) was installed and connected to the chamber to generate sub micrometre aerosols (Figure 9). The atomizer was operated in recirculation mode. The atomizer generates droplets with a number median diameter about 0.3 µm (geometric standard deviation <2), and mean particle size varies between 0.02 and 0.3 µm by atomizing a solution and evaporating the solvent. This operation mode may involve a gradual evaporation of the solvent, causing the solution in the reservoir bottle to become more concentrated. Therefore, our experiments run over short period of time. Two different types of solutions were used in the project, NaCl solution and MEA solution both at three different concentrations.

The atomizer requires connection to compressed air at 2.4 bar. Thus, pressures gauges were installed (Figure 9) to keep the compressed air pressure constant and at the required level.

The operation principle of the new fog-chamber at NILU consist of:

1. Preparation of the solution (NaCl or MEA) with the concentration of interest.
2. The humidifier is turned ON and temperature and relative humidity sensors set up for measuring or logging. These conditions are kept during one hour before we proceed with next step.
3. Fill the bottle of the atomizer about three-fourths full of the solution (i.e. NaCl or MEA).
4. The bottle is connected to the atomizer.
5. The pressure is set at 2.4 bar and the performance of the atomizer is checked before connecting to the chamber.
6. The aerosol outlet of the atomizer is connected to the chamber so that the polydisperse aerosol enters the chamber. We wait 30 minutes before we proceed further.
7. Fan is turned ON.
8. We wait 30 minutes before we start sampling droplets.
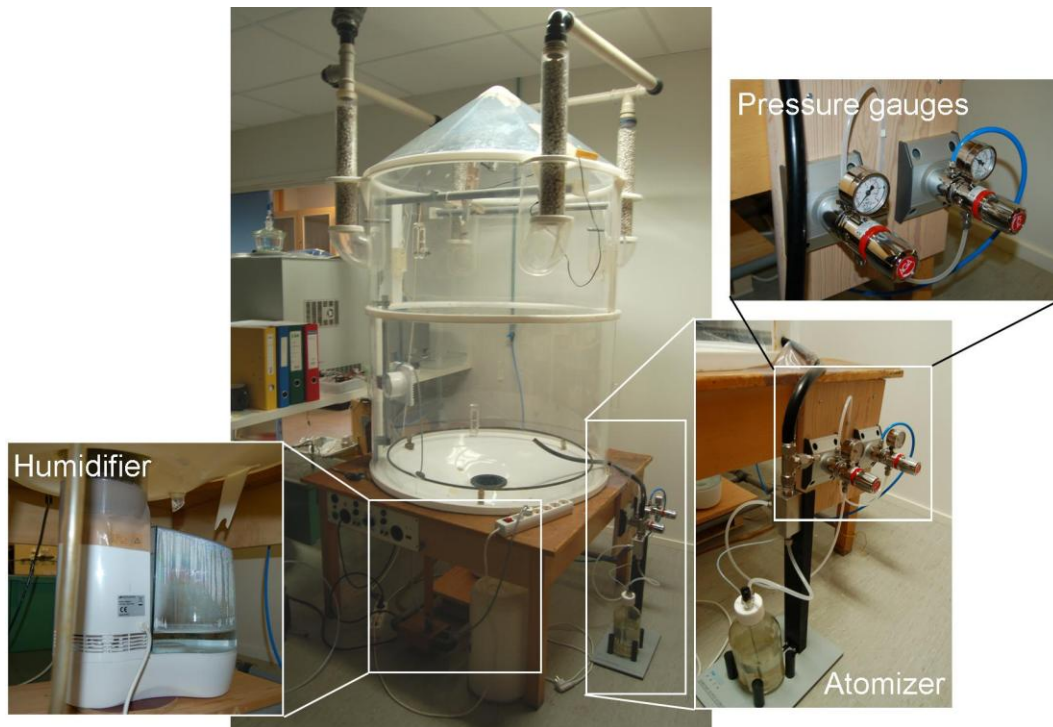
Figure 9:   Design of the fog-chamber.

The cleaning procedure after each experiment was a critical step of the experimental process. The main aim of the cleaning process was to remove possible impurities from previous experiments in order to avoid contamination. For the cleaning the aerosol droplet collector was removed. The chamber was dismantled and the inner walls of each construction element were cleaned using tissues with absolute alcohol and then tissues with water to carefully remove possible salt crusts. After the chamber cleaning a one hour run with pure water was performed.

3.3   Installation of a aerosol droplet sampler in the chamber

The aerosol droplet sampler (Sampler Model 212) was bought from John W. Hock Company (http://www.johnwhock.com/) and installed inside the fog chamber. The droplet sampler consist of a mechanical slide rotator motor designed to collect insecticide aerosol droplets on glass slides (Teflon or MgO coated), a holder for two slides and a 12 VDC celled-electrolyte battery.

The aerosol sampler was installed on the upper part of the chamber (Figure 10), positioned in the centre and attached to an aluminium bar. The original design of the sampler was modified based on the functionality observed after some experiments. The most significant modification concerned the rotation of the aerosol sampler. The original was 450 rpm, which involved exceptionally high number of overlapped impacts on the slides. In order to reduce the number of impacts, the battery was substituted for a voltage controller which was connected to the power and adjusted to obtain an approximated rotation of 100 rpm. The modification allowed us to sample long enough and to reduce the number of overlapped impacts which characterization was unfeasible.
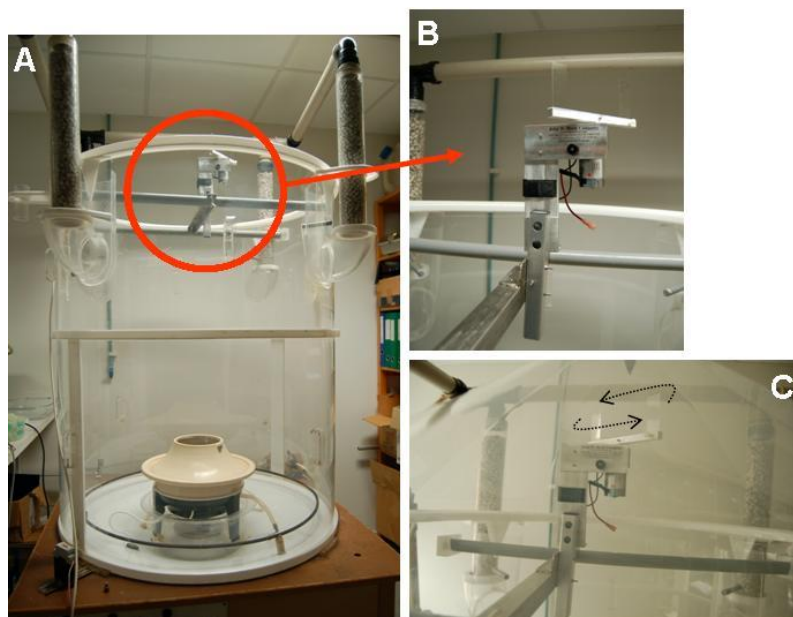
Figure 10: Installation of the droplet sampler in the fog chamber.

3.4 Control of the chamber outflow

During one hour of experiment 550±50 g water are evaporated from a solution in a bowl placed on the ground of the chamber and lost through the exhaust outlet. Repeated measurements of the air velocity, using a *TSI Air Velocity Transducer 8386-M-GB*, directly at the circular exhaust outlet (Figure 11; diameter of 5.0 cm) showed that the velocity of the air stream leaving the chamber is 1.66±0.03 m/s. Based on the measured air velocity it is calculated that the air flux out of the chamber is 11.7 m^3/hr. This implies that the whole chamber volume is replaced about 13 times per hour. Thus the residence time of vapour and droplets inside the chamber is probably around 4.8 minutes. For this reason, experiments in the chamber can only provide a momentary picture of the thermodynamic equilibrium between water vapour and droplets rather than a time series of droplet evolution. However, it can be expected that in the first 30 minutes of the experiment, a dynamic evolution can be observed due to the ongoing change of temperature and the time required to reach the equilibrium state throughout the chamber volume. Steady state calculations demonstrate that the water content inside the chamber is constant at 46.8 g after 30 minutes as an average for the experiments.

Figure 11: Flow measurements at the outlet of the fog chamber.

3.5 Control of temperature and humidity

Due to incomplete mixing of the chamber air there may exist gradients of temperature and humidity inside the chamber. Temperature and relative humidity were measured during the experiments with the available instruments and subsequently logged manually or continuously logged using a RMS Multimeter from Fluke.

Initial test experiments were performed to identify possible temperature and humidity gradients in the fog chamber. Three stages of operation were run in the test experiments: an initial warming stage (humidifier on), followed by a mixing stage (using ventilation), and a final cooling stage (humidifier and ventilation stopped). During the warming stage (first hour of the experiment), the chamber top warmed up rapidly and the chamber ground slower. In the warming stage a temperature difference of 2.5°C existed on average between top and ground (Table 3, Figure 12). After the fan was switched on, temperature and relative humidity differences became small. The chamber ground was on average 1.1°C warmer than the top and the temperature curves were parallel and increased slowly throughout the mixing stage. After both fan and humidifier were stopped, temperature dropped rapidly. In the cooling stage, relative humidity increased further though no replenishment of humid air took place. In this stage, condensed drops evaporated from the chamber walls. During the cooling stage the ground was on average 1.9°C colder than the chamber top.

Table 3:   Temperature and relative humidity during a typical three stage (1=warming, 2=mixing, 3=cooling) experiment measured at the top of the upper cylinder (=top) by a digital thermometer (Clas Ohlson, www.clasohlson.no, art. no. 36-1264) and 15 cm above ground (=grd) by a TSI Air Velocity Transducer.

Exp. Time	T(top) °C	T(grd) °C	RH(top) %	RH(grd) %	Operation	Stage
00:00	23	–	21	–	Start humidification	1
00:30	30	–	95	–	–	1
00:45	31	–	95	–	–	1
01:00	31	28.0	95	92.8	TSI sensor inserted (grd)	1
01:10	30	31.2	96	95.9	Fan on	2
01:40	30	31.2	96	95.9	(wall covered with drops)	2
01:47	29	27.0	96	94.9	Fan and Humidifier stopped	3
01:53	27	23.7	96	95.1	–	3
02:40	22	21.7	98	98	(wall clears partly)	3
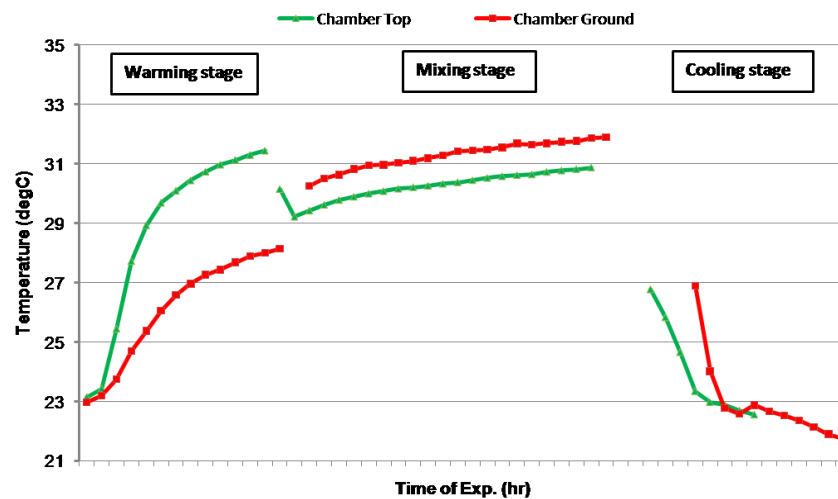
Figure 12: Logged time series of the air temperature inside the chamber on 08.04.2010 and 09.04.2010, measured at the top of the upper cylinder (chamber top) and 15 cm above the ground (chamber ground). Some data points were removed to display the different stages more clearly. Measured temperatures are from two different experiments, but the graph illustrates differences during typical experimental procedure.

Air pressure in the chamber was not measured because an appropriate sensor was lacking. It is assumed that there occurs a pressure drop during the experiment. An indication for this is that temperature at the ground falls below the laboratory temperature at the end of the experiment. Without pressure measurements it is not possible to tell whether the experimental design followed the adiabatic cooling of an air parcel.

We recommended to install a pressure sensor, together with a dew point hygrometer, and a logging humidity sensor in future experiments with the fog chamber.

A typical temperature profile during an experiment is shown in Figure 13. A temperature drop from 32°C to 30°C occurs when the ventilation is switched on (at 15:00). With ventilation on, temperature remains stable between 30 and 31°C throughout the remaining experiment time. Little deviation (<0.3°C) is found between the maximum and minimum temperature value recorded during a 5-minute measurement interval.

Temperature 18.05.2010
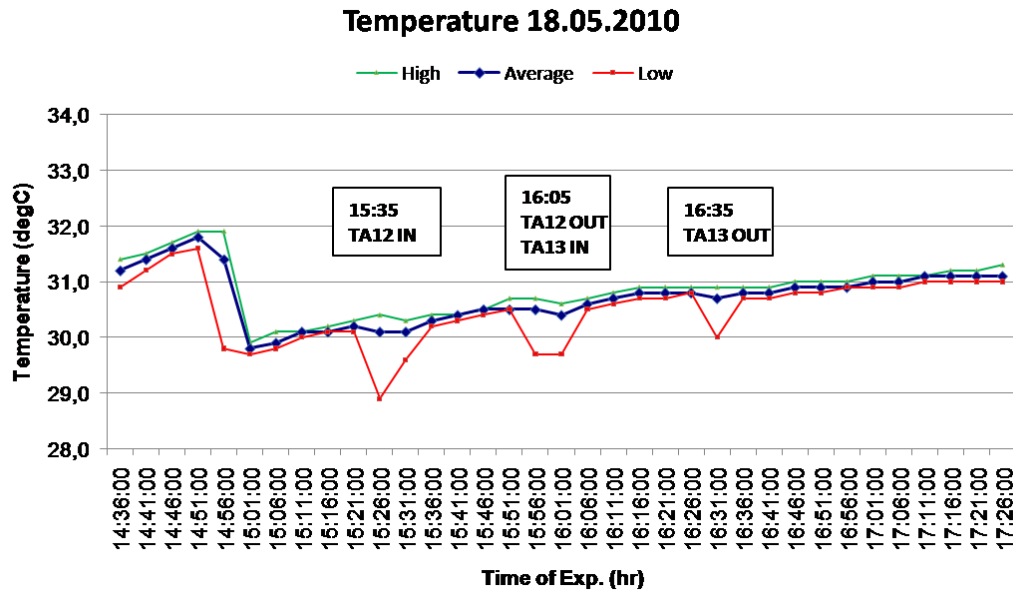
Figure 13: Logged time series of the air temperature inside the chamber during the experiment on 18.05.2010. Green and red line indicate temperature maximum and minimum values, respectively, during a 5-minute measurement interval.

Short-term (5-10 minutes) temperature drops are noted for the times when the droplet collection slides were inserted or exchanged. For this procedure the chamber roof had to be lifted for 1-2 minutes. The average temperature during a 5-minute interval was not affected by this procedure.

3.6   Calculation of expected supersaturation

A rough estimate of the supersaturation in the fog chamber experiments can be derived for a steady state situation. We presume that a steady state for the water vapour saturation ratio within the chamber was reached at least after half an hour, i.e. when the chamber air temperature became roughly constant. Condensation of water vapour to the droplets is the dominant growth process, while sedimentation and coalescence during the experiments are not relevant since relatively small droplet sizes were found (<25 μm). The ambient saturation ratio inside the chamber will thus control the condensation process.

We assume that vapour is provided by saturated air that is cooled in the ascent (on its way from the humidifier at the chamber ground to the chamber outlets) and that vapour is lost by condensation on the growing droplets. Then the rate of change of the saturation ratio S can be written as:

$$\frac{dS}{dt} = P - C \tag{16}$$

Where P denotes a production term and C is a condensation term. More specifically, it is:

$$\frac{dS}{dt} = Q_1 \frac{dz}{dt} - Q_2 \frac{d\chi}{dt} \tag{17}$$

Where dz/dt is the vertical air velocity (measured in section 3.4) and $d\chi/dt$ is the rate of condensation measured in terms of condensate per mass of air per unit time. Q_1 and Q_2 are thermodynamic variables. A limiting, steady state value of supersaturation s can be derived from Equation (17) when assuming that the droplets are large enough in order to neglect the solution and curvature terms in the droplet growth equation and that all droplets are of same radius r (Rogers and Yau, 1989):

$$\frac{ds}{dt} = \omega - \eta s \tag{18}$$

Where $\omega = Q_1 U$ and $\eta = 4\pi\rho_L v_0 r Q_2/(F_k + F_d)$, with the vertical air (updraft) velocity U (in m/s), Q_1 in 1/m, radius r in m, the droplet concentration ρv_0 (in #/m^3), Q_2 (in kg/kg). F_k represents a thermodynamic term associated with heat conduction and F_d is the term associated with vapour diffusion. The limiting value of the supersaturation (for ds/dt=0) is:

$$s(\%) = \frac{\omega}{\eta} \cdot 100 \tag{19}$$

The terms ω and η can be regarded as constant because they are slowly varying compared to s. In our experiments the average droplet radius varied between 5 and 15 μm, estimated droplet number concentrations were between 100 and 1200 #/m^3, and pressure probably ranged between 80 kPa and standard pressure. For the given conditions the limiting value of supersaturation in the experiments is calculated to be between 0.01 and 0.3% according to Equation (19). The estimate provides some confidence that slightly supersaturated conditions were achieved in all experiments.

4 Quantification of impacts by using image processing

The methodology for the quantification and characterization of droplet impacts during the experiments has been developed in the project. As it was explained in previous sections, the droplet sampler was installed and adapted into the fog-chamber. MgO-coated glass slides were adjusted to the droplet sampler and used as substrate to register the impacts of the droplets during the experiment. The droplet impact prints are approximately circular "craters" which are registered on the MgO coating. Once the experiments finalized, the slides were immediately brought to the microscope for their evaluation.

The glass slides were analyzed by optical microscopy using a *Leitz Aristoplan* microscope. Digital images for the quantification and characterization of impacts where taken using a *Leica DC Camera* attached to the microscope and with the help of *Leica IM Management system*. In order to perform an accurate evaluation of the droplet impacts on the coated glass slides and assess the method, two different types of digital images were taken during a testing period of the fog-chamber. Images from transmitted and reflected light conditions were taken in order to evaluate the difference and determine the best method to quantify droplet impacts. Figure 14 shows the difference between images taken under reflected and transmitted light conditions.
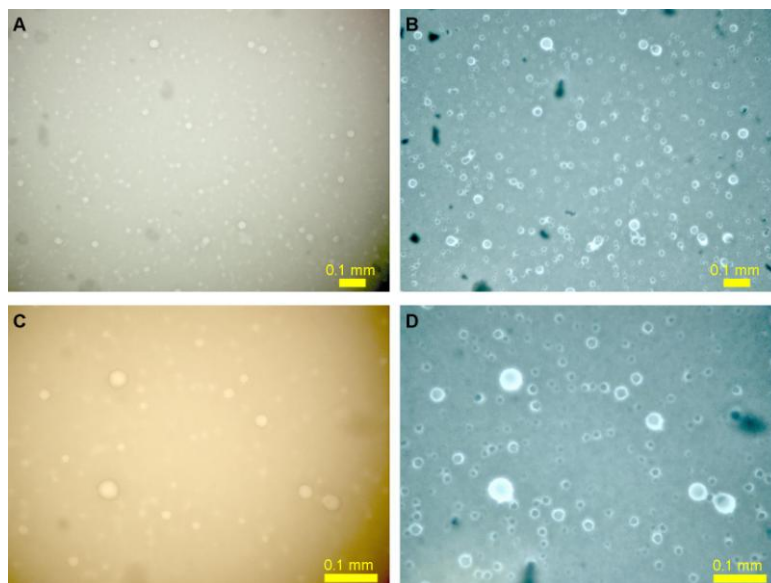
Figure 14: Reflected and transmitted light images. Image A and B represent the same area of the coated glass slide under reflected and transmitted light conditions, respectively. C and D shows the same area under reflected and transmitted light, respectively.

Under reflected light conditions images are homogeneous (Figure 14) facilitating the quantification and characterization of impacts. The images taken under transmitted light conditions show colour heterogeneities (Figure 14), which involve an intensive image processing previous to the quantification. However, the number of impacts observed under transmitted light conditions is higher than the number of impacts observed under reflected light. As a consequence, transmitted light image are difficult to process but they represent more accurately

the experiment. Under reflected light conditions, some impacts are not observed and therefore the quantification may be underestimated. All the results presented in this report were obtained after the analysis of images taken under transmitted light conditions.

Images were analyzed by the image processing freeware software *ImageJ*. The image processing and the steps preceding the quantification depend on the type of image. The main aim of the image processing is to obtain a homogeneous binary image (Figure 15). Different steps such as modification of brightness and contrast, application of filters, adjustment of manual thresholds, and transformation to 8-bits image are followed.

The common quantified parameters are percentage of area covered with impacts, size and dimension of each impact and circularity. In order to quantify only single impacts and avoid overlapping, the quantification is limited to certain size of impacts prints and high circularity.
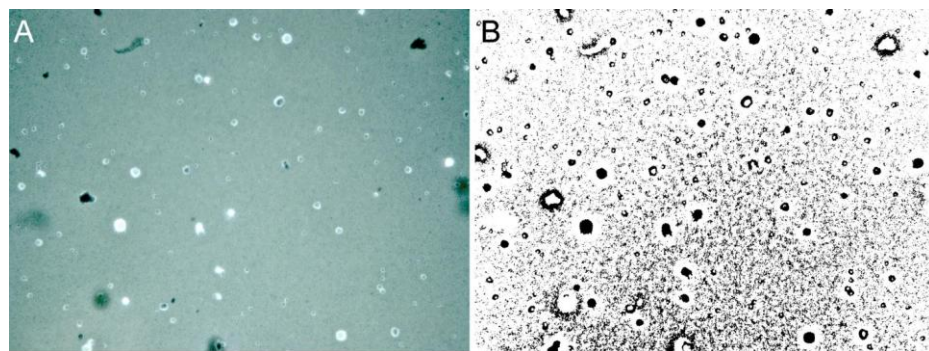
Figure 15: Digital image taken form a glass slide exposed in the fog-chamber (A) and its corresponding binary image (B).

For the characterization of impacts the study focused on two main parameters, the area of the impact print and the diameter. The diameter was obtained both as Feret diameter and from the major axis of the best fit ellipse to the crater with the same area. The Feret diameter was the main parameter used in the evaluation of the results to characterize the droplet impact. The Feret diameter is the distance between two tangents on opposite sides of the crater profile, that are parallel to some fixed direction. The Feret diameter is usually used in visual microscope counting. Another parameter taken into account was the circularity. This parameter varies from 0 and 1, corresponding to a very elongated object and a perfect circle, respectively. The circularity was used as a filter parameter in the analysis of impacts, as the quantification was limited to those impacts with high circularity values and therefore avoiding impacts which were the results of overlapping of different droplets.

The methodology developed in the project for counting and characterizing impact prints is time consuming and, based on the experience achieved in the project, involve certain uncertainties. Therefore and for further studies, it is advisable to install a droplet counter.

5 Results from fog chamber experiments

Table 4 summarizes the experiments performed in the project. Three types of experiments were performed with NaCl and monoethanolamine (MEA) solutions in water at 0.6, 2.6 and 5.3 wt-% (percentage of weight) concentrations. Each experiment was performed two or three times consecutively in order to evaluate the reproducibility of the experiments and possible temporal variations of the fog chamber performance.

Table 4:   Experiments performed in the project with NaCl and MEA solution at different concentrations.

# Run	Solution	Concentration (%)	Exposure (min)	Date (dd.mm.yy)
TA8	NaCl	0.6	30	26.04.10
TA9	NaCl	0.6	30	26.04.10
TA2	NaCl	2.6	30	22.04.10
TA3	NaCl	2.6	30	22.04.10
TA4	NaCl	2.6	30	22.04.10
TA5	NaCl	5.3	30	23.04.10
TA6	NaCl	5.3	30	23.04.10
TA7	NaCl	5.3	30	23.04.10
TA10	MEA	0.6	30	28.04.10
TA11	MEA	0.6	30	28.04.10
TA12	MEA	2.6	30	18.05.10
TA13	MEA	2.6	30	18.05.10
TA14	MEA	5.3	30	19.05.10
TA15	MEA	5.3	30	19.05.10
TA16	MEA	5.3	15	19.05.10

5.1 Reproducibility of experiments

Appedix A shows the average results obtained in the experiments performed as part of the project. Two or three experiments were performed with the same solution concentration in order to evaluate the reproducibility of the experimental results. The experiments were performed consecutively, the same day, keeping certain time interval between experiments (≈30-45 minutes), and using the same solution in the aerosol atomizer. The comparison of the results shows a certain similitude and when differences are found, they are due to the quantification process.

For the evaluation of the results and the study of droplet formation, one experiment of each type was selected based on criteria which guaranty the accuracy of the results. Among the criteria selected are the quality of the image, feasibility of the quantification and accuracy of the quantification based on evaluations performed during the image and quantification processing.

5.2 Droplet distribution with sodium chloride solution

Figure 16 shows different magnification of images from the droplet impact prints obtained with NaCl solution at 0.6, 2.6 and 5.3 wt-% concentrations. From the visual evaluation of the image it is possible to establish an increase in number of impact with concentration. The image from the experiment performed at 5.3 wt-% of NaCl shows higher number of impact and in addition they seem to overlap significantly. The experiments performed with the lowest concentration in NaCl (i.e. 0.6 wt-%) seems to show fewer impact prints. The visual evaluation is supported by the results obtained by quantification of impact prints. The lowest number of impact prints obtained on a surface of 8.26 mm^2 is achieved in the experiment at lowest concentration of NaCl, whereas higher NaCl concentration gives higher number of impacts (Table 5 and Figure 17).

Table 5: *Number of impacts obtained in the experiments performed with solution of NaCl.*

Experiment	NaCl (wt-%)	# impacts
TA9	0.6	4 870
TA4	2.6	10 050
TA7	5.3	7 862

The experiment performed with the 5.3 wt-% NaCl solution seems to show lower number of impact than those obtained with 2.6 wt-% NaCl solution. The reduction in impact print circularity for the 5.3 wt% splution indicate a higher number of impact overlaps. A high number of overlaps will increase the uncertainty in the image analysis.

Table 6: *Average, Standard deviation and median area, circularity (Ci) and diameters expressed as Major best fit ellipse (Major) and Feret diameter. C: concentration expressed as %.*

	C (%)		Area (µm^2)	Ci	Major (µm)	Feret (µm)
TA9_x10	0,6	average	31,93	0,78	8,04	8,80
		st. dev.	14,64	0,12	1,85	1,97
		median	27,55	0,80	8,00	8,00
TA4_x10	2,6	average	40,39	0,78	8,78	9,60
		st. dev.	39,82	0,12	2,88	3,02
		median	31,74	0,80	8,00	9,00
TA7_x10	5,3	average	37,24	0,74	5,24	9,47
		st. dev.	32,25	0,13	1,66	2,75
		median	29,26	0,75	5,00	9,00

In addition to the number of impact detected on coated glass slides, the size of the impact was quantified and evaluated. The average and media in area results show a slightly increase with the concentration of NaCl in the solution employed in the experiments (Table 6 and Figure 17) although the differences are not significant. The average diameter of the impacts prints in the three selected experiments is around 10 µm (Table 5 and Figure 17) what is consistent with the mean cloud droplet size (Figure 6).

Summary of the results obtained from the experiments with NaCl solution:

- *The lowest number of impact is obtained with the least concentrated sodium chloride solution (i.e. 0.6% NaCl).*
- *High number of impacts which involves high overlapping was obtained with the highest concentration of NaCl (i.e. 5.3%).*
- *The highest number of impact for all the experiments performed with NaCl seems to show a diameter between 8 and 10 μm.*
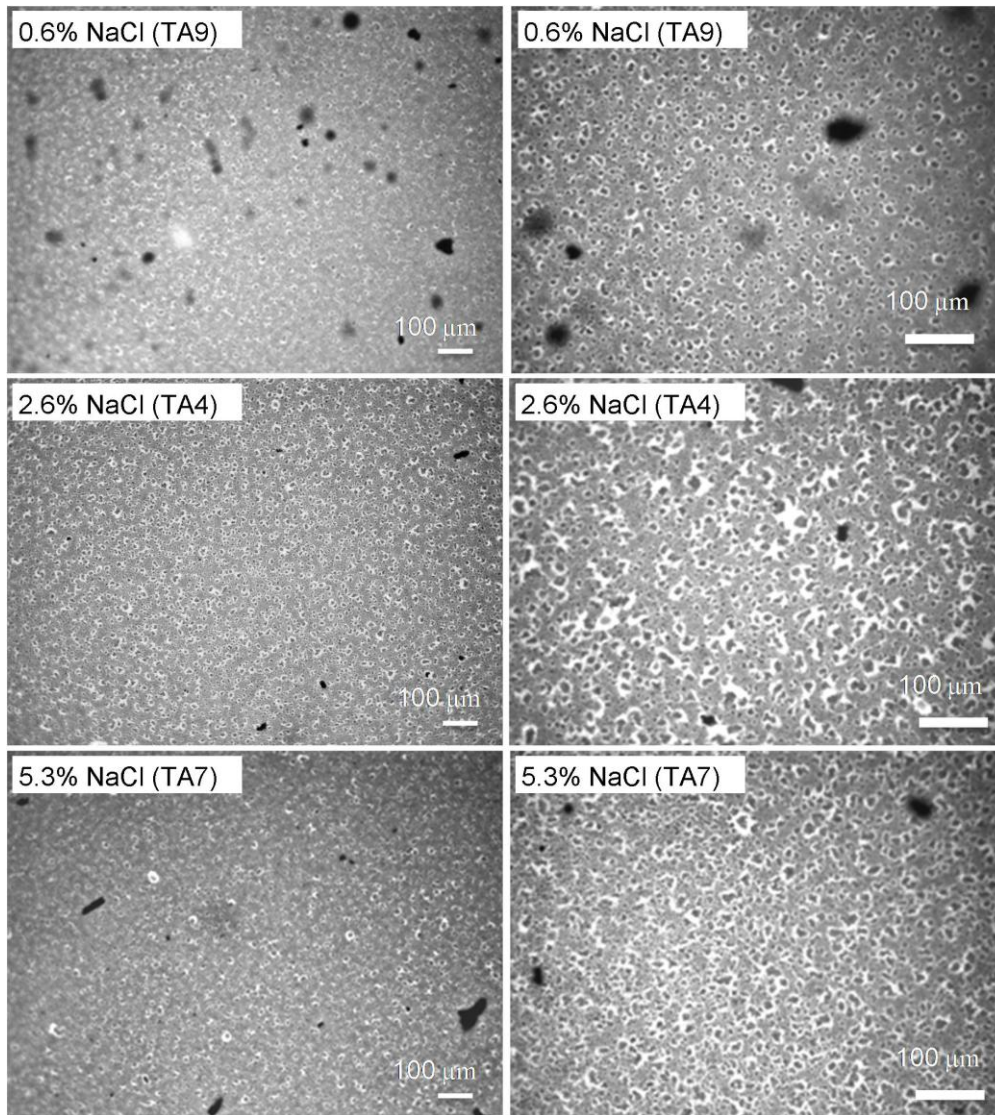
Figure 16: Droplet impacts on MgO-coated glass slides exposed in the fog-chamber with different NaCl aerosol concentrations. Exposure time: 30 minutes each experiment.
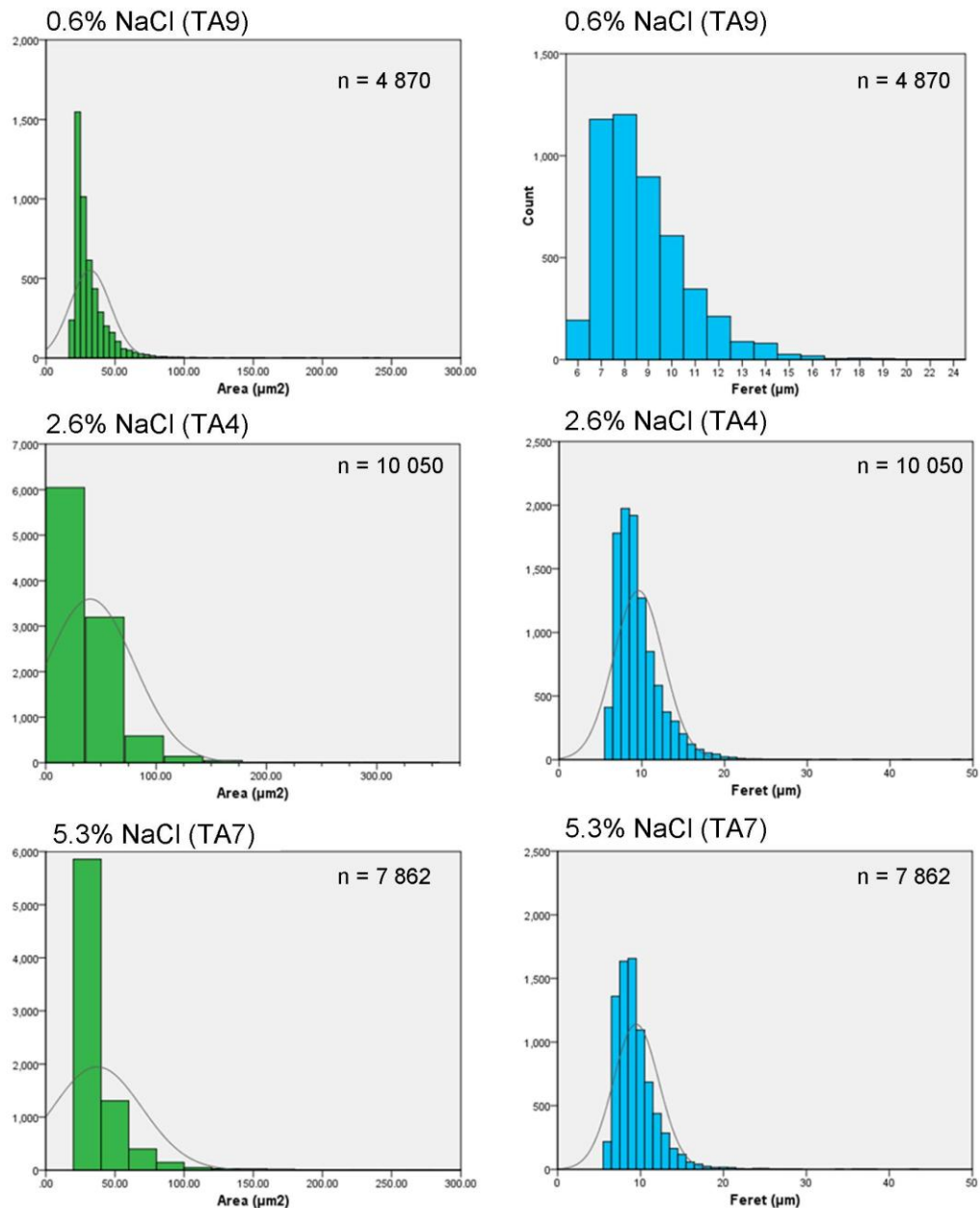
Figure 17: Area and diameter (Feret) distribution of impacts prints over a study area of 8.26 mm2 obtained under different NaCl aerosol concentration.

5.3 Droplet distribution with MEA solution

Three different types of experiments were performed with monoethanolamine (MEA) solutions at three different concentrations, 0.6, 2.6, and 5.3 wt-% (Table 4). Figure 18 shows the images of the droplet impacts prints for each concentration at two different magnifications. The visual evaluation and comparison of the images obtained with NaCl show a significant difference between the two compounds (Figure 16 and Figure 18). Two families of droplet impacts prints are observed in the experiments performed with MEA solution (Figure 18) as larger impacts than those obtained with NaCl are easily identified from the images.
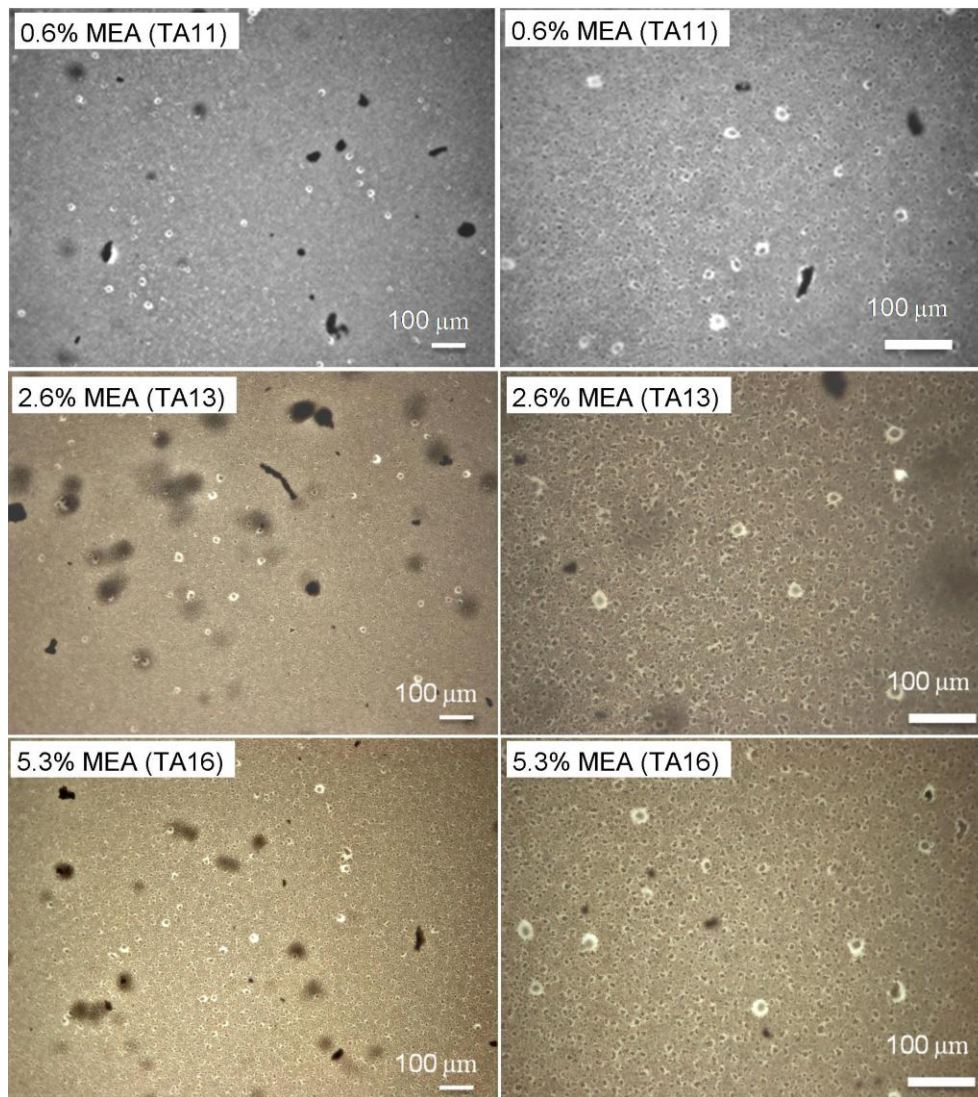
Figure 18: Droplet impacts on MgO-coated glass slides exposed in the fog-chamber with different aerosol concentrations of MEA. Exposure time: 30 minutes (TA11 and TA13)and 15 minutes (TA16).

The different families of impact prints are observed on the area and diameter distribution, where bimodal distribution is obtained (Figure 19). One of the populations shows an area around 40 μm^2 and diameter approximately 8 μm, whereas the other family, although less abundant (Figure 18), reach an area around 300 μm^2 and approximate diameter of 25 μm. The two families of impact prints is obtained under the three MEA solution concentrations (Figure 18 and Table 7).

One of the most significant results is with regard to the amount of impact. The experiment performed with 5.3 wt-% MEA solution showed such amount of impacts that the experiment had to be repeated at shorter exposure time. The amount of impacts was so large that the identification of impact prints was not possible. The experiment was performed at 15 minutes exposure time, half of the time used for the rest of experiments. The obtained results supported previous

findings concerning the appearance of two families of impact prints. However, even if the visual evaluation of the images was possible, the quantification was not due to a high deterioration of the slides MgO-coating. The acquisition of digital images with suitable quality for processing and quantification was not possible. These difficulties were previously pointed out and support the need of a droplet counter for further studies with the NILU fog-chamber.
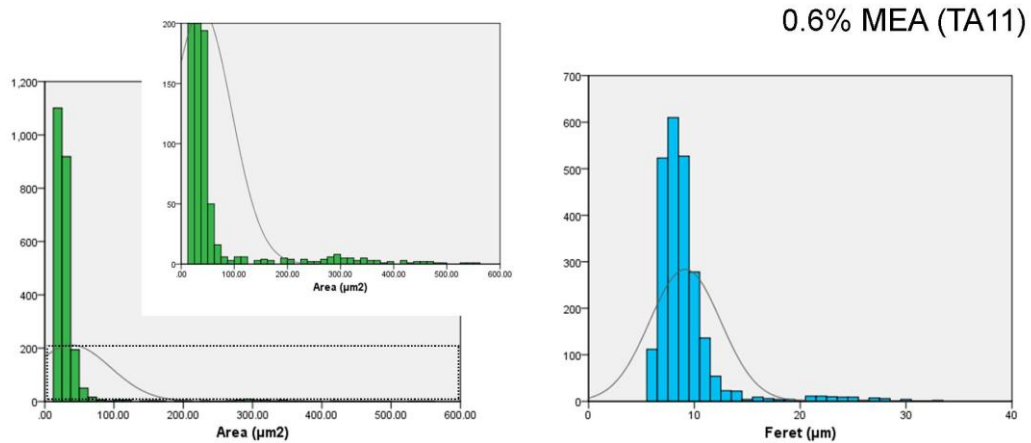
Figure 19: Area and diameter (Feret) distribution of impacts prints over a study area of 8.26 mm^2 obtained under at 0.6 wt-% of MEA solution.

Table 7:   Average, Standard deviation and median area, circularity (Ci) and diameters expressed as Major best fit ellipse (Major) and Feret diameter. C: concentration expressed as wt-%.

	C (%)		Area (µm²)	Ci	Major (µm)	Feret (µm)
TA11_x10	0,6	average	38,62	0,75	8,25	9,13
		st. dev.	56,29	0,13	3,05	3,36
		median	25,79	0,76	8,00	8,00
TA13_x20	2,6	average	109,44	0,67	11,67	11,67
		st. dev.	196,33	0,02	8,98	8,98
		median	29,52	0,67	7,00	8,00
	5,3	average	n/a	n/a	n/a	n/a
		st. dev.				
		median	n/a	n/a	n/a	n/a

6 Implications of the experimental results for the growth of cloud droplets under atmospheric conditions

The droplet population evolving in the fog chamber can be compared to the droplet population within a rising air parcel. The features of such a droplet population have been described by Howell (1949):

1. The initial population of solution droplets which form from deliquescent aerosol particles will grow in sub-saturated conditions as the relative humidity inside the air parcel increases. This can be observed in the first half an hour of the experiment in the fog chamber, when the polydisperse wet aerosol particles generated by the Atomizer enter the chamber and grow in sub-saturated conditions.
2. As relative humidity exceeds 100%, the larger droplets activate (by exceeding the critical size) and form first cloud/fog droplets.
3. A maximum supersaturation is reached which represents a balance between moisture available for condensation and the growth of cloud/fog droplets.
4. Cloud droplets can be turned into haze droplets when the supersaturation of the air parcel is reduced to a value below the equilibrium supersaturation for a time long enough to shrink cloud droplets to haze size.
5. Certain droplets of the population with critical supersaturation greater than or equal to the maximum supersaturation remain *unactivated*, or remain haze droplets, i.e. they don't grow further. This is expected to take place in the fog chamber experiments as well, however with the current instrumentation it is not possible to distinguish between activated and *unactivated* droplets. For this a CCN counter combined with an instrument to measure the full droplet size distribution would be required.

The critical supersaturation in the air parcel will be affected by the solute (NaCl or MEA) through the solution effect (Raoult) and/or the curvature effect (Kelvin). While NaCl will affect the equilibrium saturation ratio only through the solution effect described by Raoult's law, MEA could have both effects from which the Kelvin effect would be of greater importance since it determines the possibility for the very small droplets to grow. To evaluate the theoretical consequence that the presence of both compounds have for droplet growth, the basic Köhler equilibrium model outlined by Karl (2008) was applied.

It is noted that the effect of dissolved NaCl ions (Na$^+$, Cl$^-$) on surface tension was considered according to (Jacobson, 2005):

$$\sigma_p = \sigma_{w/a} + 1.7 \cdot m_I \tag{20}$$

Where σ_p is the surface tension of the particles (g s^{-2}), $\sigma_{w/a}$ is the surface tension of water at the respective temperature and m_I is the molality of the sodium ion plus that of the chloride ion (which equals twice the molality of undissociated NaCl), assuming that dissolved NaCl is fully dissociated. The effect of dissolved inorganic ions is to increase the surface tension of water droplets and thus to increase the saturation vapour pressure of water over a curved surface.

The effect of dissolved MEA on surface tension is determined using the empirical Szyszkowski-Langmuir equation for dissolved organic carbon as given by Facchini et al. (1999):

$$\sigma_p = \sigma_{w/a} - 0.0187 \cdot T \ln(1 + 628.14 \cdot m_C) \tag{21}$$

Where m_C the molality of carbon dissolved in water (mol C kg_{H2O}^{-1}). Particle surface tension is determined according to Eq. (21) for a given molality of carbon from dissolved MEA.

Figure 20 shows the calculated Köhler curves obtained from the model for NaCl and MEA at different concentrations. For both compounds the Köhler curve for lowest concentration of 0.6 wt-% is dominated by the curvature effect (Kelvin) while for the highest concentration of 5.3 wt-%, the solution effect (Raoult) prevails. The critical radius calculated for the NaCl and the MEA aerosol is rather similar (Table 8). However, the critical supersaturation required to activate the droplet population is substantially lower for the MEA aerosol than for the sodium chloride aerosol (Table 8). The difference in critical saturation ratios is most obvious for the 2.6 wt-% solutions (Figure 20) because these curves show a clear maximum (between 0.030 to 0.040 μm droplet radius). For this concentration, critical supersaturation is 2.06% for the NaCl solution while it is only 1.59% for the MEA solution. This implies that at an ambient supersaturation of 1.8% the droplet population generated from the MEA solution can be completely activated while for the NaCl solution only those droplets with radius larger than ~0.060 μm become activated. The reason for the lower critical saturation ratios of MEA solutions compared to NaCl solutions of same concentration is the effect of dissolved MEA (organic carbon) on surface tension. The addition of dissolved organics (organic carbon) to water droplets decreases the saturation vapour pressure and reduces the effect of curvature. Since the curvature effect dominates the saturation ratio curves at low concentrations, the reduction of surface tension in droplets containing dissolved MEA compared to those containing dissolved NaCl is most pronounced, in particular for small droplet sizes (compare blue lines in Figure 20a and b).

a)   b)
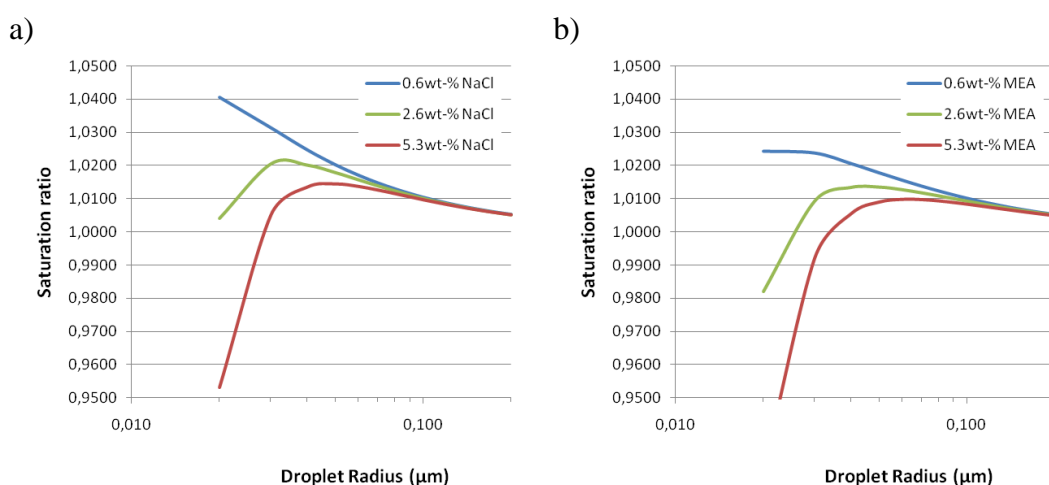
Figure 20: Köhler curves calculated from the equilibrium model (Karl, 2008) for different a) NaCl and b) MEA concentrations (wt-%).

40

Table 8: *Critical radius and saturation ratio obtained from the Köhler model (Karl, 2008) for different NaCl and MEA concentrations.*

C (wt-%)	NaCl		MEA	
	r* (µm)	S*-1 (%)	r* (µm)	S*-1 (%)
0.6	0.017	4.16	0.017	3.72
2.6	0.034	2.06	0.037	1.59
5.3	0.049	1.44	0.054	1.01

The increasing number of impacts/droplets with increased concentration of solute observed in the fog chamber experiments (overlapping impacts obscured number counting for the highest concentration, but numbers were visually the highest) can only be explained with the enhanced activation of small droplets when the concentration of solute was increased. Other explanations can be ruled out since the particle number concentration generated by the constant output atomizer as well as average chamber temperature and humidity were very similar in all experiments. Only the activation of more small droplets could have provided additional numbers of droplets which could grow further by condensation. Model results indicate that supersaturation in the fog chamber was probably between 1 and 2% in order to allow for activation of smaller droplets (below 100 µm radius), at the higher concentrations of solute, which is higher than the estimated supersaturation derived in section 3.6 (0.01 to 0.3%). The reason for the too low estimate derived from steady state considerations and using realistic values for average temperature, pressure, droplet number concentration, and droplet diameter in the experiments is likely the neglect of the solution and curvature terms when estimating the steady state value of supersaturation (Equation (18) in section 3.6).

Though the residence time of air (and probably also water droplets) in the fog chamber is less than 10 minutes as determined in section 3.4, the time period was long enough to allow small droplets to grow into µm-sizes by condensation. This is supported by Table 1, which displays the time necessary for the growth of a 0.75 µm droplet containing 10^{-14} g NaCl at 0.5% supersaturation. The time required to grow to 10 µm (radius) is only 2700 s in this example. The diameter range obtained for the final fog droplet populations in the experiments with NaCl and MEA between 5 and 20 µm agrees well with the diameter range observed for atmospheric fogs.

Interestingly, the droplet population generated from MEA solutions showed a second mode of larger droplets between 20-30 µm diameter size. An explanation for this finding is that droplets initially forming on a larger nuclei passed the barrier (critical radius) at an early stage of the experiment and grew faster than others - on cost of the droplets that formed on the smaller nuclei - and were turned into the observed larger droplets of 20-30 µm diameter. Since these larger droplets were not observed in the experiments with NaCl solution, it is concluded that the saturation ratio for droplets of the same radius (e.g. 0.06 µm) must have been

lower in the MEA experiment than in the NaCl experiment with the same concentration.

This finding together with the unexpectedly high amount of impacts for the 5.6 wt-% MEA solution support the earlier conclusions obtained from a Köhler equilibrium model (Karl, 2008) and those derived with the model in this work, that dissolved MEA 1) effectively depresses surface tension of water droplets, 2) allows for activation of smaller droplets at lower ambient supersaturation, 3) enhances the number of droplets that become activated with increasing solute concentrations more efficiently than NaCl, and 4) enables faster growth of small droplets into larger droplets/drops.

Implications for the atmosphere. The presence of dissolved MEA in small water droplets will lower their surface tension and in consequence allow for growth out of the equilibrium state at lower ambient supersaturation compared to pure water droplets or droplets containing equal amounts of sodium chloride. Dissolved MEA enhances the probability that very small water droplets can grow to fog/cloud droplet size (10-20 µm) and cause fog or cloud formation. Because of the surface tension depression resulting from dissolved MEA, cloud droplets can grow to larger droplets that can form rain drops. In the atmosphere, growth from cloud droplet sizes (10 to 20 µm) to rain drop sizes (several hundred µm to 2 mm) not only occurs by water vapour condensation but also by coalescence of droplets and ice-related processes. To study how dissolved MEA affects the possibility of rainfall and the amount of rain water for certain meteorological conditions the development and application of a microphysical aerosol/cloud model is necessary.

7   Further improvements and recommendations

There are some remaining issues that should be elaborated in more detail to proceed with studies on droplet growth in the NILU fog chamber. First, some further technical improvements, including the acquisition of new instruments, are necessary. Second, open research questions were identified for the possible future use of this new facility.

Technical improvements:

1. A droplet size measurement instrument (based on optical principles) should be acquired to follow the temporal evolution of the size spectrum of the droplet population. This would allow for a more reliable evaluation of the droplet growth processes and droplet number concentrations. In first instance the instrument can be used to evaluate results simultaneously obtained with the aerosol droplet collector.
2. A diffusion dryer and a neutralizer should be acquired as additional equipment for the constant output atomizer in order to generate a better defined initial aerosol.
3. A pressure sensor, together with a dew point hygrometer, and a logging humidity sensor should be installed to better characterize the saturation ratio in experiments.
4. Installation of a pulley tackle to lift the upper cylinder of the fog chamber.

Open research questions:

1. *Surface tension measurements*. Experimental data on surface tension of solutions of MEA and other soluble organics should be acquired in lab experiments and fit to the Szyszkowski-Langmuir. Pendant drop tensiometry (PDT) is a technique commonly used to measure surface tension in complex mixtures (Adamson and Gast, 1997).

2. *Gas-phase reservoir of surface-active organics*. Uptake of gas phase compounds may affect the activation of aqueous aerosol. Theoretical considerations on the uptake of gas-phase MEA to aqueous aerosol particles and droplets revealed the possibility of MEA to affect the activation of a droplet population and number concentration of CCN. Recent preliminary results show that acetaldehyde and formaldehyde are additional sources of surface tension depression in aqueous aerosols (McNeill et al., 2010). Karl (2008) assumed that the partitioning of amines between the gas phase and the aerosol water is determined by the thermodynamic equilibrium (Henry's law). Mass transfer through the air-water interface may limit the uptake of gases to the aerosol particles.

3. *Droplet activation and growth*. The fog chamber could be used as a facility to determine the potential of soluble organics to activate droplets. Droplet number size distributions during the fog chamber experiments should be monitored using a modern optical droplet measurement instrument. Results from the fog chamber method could allow for a ranking of organic compounds with respect to their ability to activate fog droplets.

4. *Development of a microphysical aerosol/cloud model*. Implementation of dynamic droplet growth following Köhler-type activation into the sectional multicomponent aerosol box model, MAFOR (Marine Aerosol Formation model), which couples aerosol dynamics with photochemistry (Karl et al., 2010). Surface tension of cloud and fog droplets containing organics should be described by the Szyszkowski-Langmuir equation and the empirical parameters obtained from lab experiments. Measured sequential droplet size distributions obtained from the fog chamber experiments can then be simulated using the model to test parameterizations for the description of droplet growth and activation.

5. *Effect of amines on rainfall probability*. To predict the possibility of rainfall and the amount of rain water for certain meteorological conditions the microphysical aerosol/cloud model (see point 4) should be coupled with a meteorological dispersion model. The meteorological model can either be a simple air parcel model, a plume dispersion model or a one-dimensional column model.

8 Conclusions

The fog chamber is a newly developed facility where characteristics of droplets in a fog generated by activation of a defined deliquescent aerosol by adiabatic cooling of a moist air volume can be studied in a reproducible manner.

A constant output atomizer was used to continuously produce wet aerosol particles from a water solution of the respective soluble organic or salt. An aerosol droplet collector was used to sample droplet impacts on MgO-coated microscope slides which were subsequently analyzed using an optical microscope. Statistical interpretations of the droplet distribution were obtained using digital image processing software. The method had limitations for high numbers of collected droplets where overlapping impacts obscured the interpretation.

Number of impacts collected on the slides increased with increasing concentration of solute while the average diameter of the observed droplet population remained fairly constant between 8 and 10 μm (Feret diameter).

Experimental results for NaCl and MEA solutions are in qualitative agreement with theoretical predictions from Köhler theory. An increase of impact/droplet numbers with increasing concentration of the solute can only be explained by the activation of smaller droplets and their subsequent rapid growth by condensation to sizes >7 μm diameter.

Addition of MEA decreases surface tension of the droplets and thus allows for the activation of small droplets (<0.20 μm) at a lower supersaturation compared to pure water droplets or droplets containing equal amounts of sodium chloride.

Impacts collected in experiments with MEA solution exhibited a weak bimodal distribution showing an additional mode of larger droplets with a diameter between 20 and 30 μm.

In atmospheric conditions, these larger fog/cloud droplets (20-30 μm diameter) eventually continue to grow and become collector droplets, when sufficient humidity is available in the surrounding air for prolonged time periods, and start to fall. Thus we speculate that amines added to atmospheric cloud water could act as a trigger of rainfall from these clouds.

9 References

Adamson, A.W. and Gast, A.P. (1997). Physical chemistry of surfaces. 6th ed. New York, Wiley.

Águila-Hernández, J., Trejo, A. and Gracia-Fadrique J. (2001) Surface tension of aqueous solutions of alkanolamines: single amines, blended amines and systems with nonionic surfactants. *Fluid Phase Equilibr.*, *185,* 165-175.

Águila-Hernández, J., Trejo, A., García-Flores, B. E. (2007). Surface tension and foam behavior of aqueous solutions of blends of three alkanolamines, as a function of temperature. *Colloids and Surfaces A: Physicochem. Eng. Aspects, 308*, 33-46.

Asa-Awuku, A. and Nenes, A. (2007). Effect of solute kinetics on cloud droplet formation: Extended Köhler theory. *J. Geophys. Res.*, *112,* D22201, doi:10.1029/2005JD006934.

Facchini, M.C., Mircea, M., Fuzzi, S. and Charlson, R.J. (1999) Cloud albedo enhancement by surface-active organic solutes in growing droplets. *Nature, 401*, 257-259.

Gill, P.S., Graedel, T.E. and Weschler, C.J. (1983) Organic films on atmospheric aerosol particles, fog droplets, cloud droplets, raindrops, and snowflakes. *Rev. Geophys., 21,* 903-920.

Gultepe, I., Tardif, R., Michaelides, S. C., Cermak, J., Bott, A., Bendix, J., Müller, M. D., Pagowski, M., Hansen, B., Ellrod, G., Jacobs, W., Toth, G. and Cober, S. G. (2007) Fog research: A review of past achievements and future perspectives. *Pure Appl. Geophys.*, *164,* 1121-1159.

Hitzenberger, R., Berner, A., Kasper-Giebl, A., Löflund, M. and Puxbaum, H. (2002) Surface tension of Rax cloud water and its relation to the concentration of organic material. *J. Geophys. Res., 107D,* 4752, doi:10.1029/2002JD002506.

Holets, S. and Swanson, R. N. (1981) High-inversion fog episodes in Central California. *J. Appl. Meteorol., 20,* 890-899.

Houghton, H.G. and Radford, W.H. (1938) On the measurement of drop size and liquid water content in fogs and clouds. *Papers Phys. Ocean. Meteorol., 6,* 4, 1-31.

Howell, W. E. (1949) The growth of cloud drops in uniformly cooled air. *J. Meteorol.*, 6, 134-149.

Jacobson, M. Z. (2005) Fundamentals of atmospheric modeling. 2nd ed. Cambridge, Cambridge University Press.

Karl, M. (2008) Amines and rainfall. Impact of amines on rainfall from plume clouds. Kjeller (NILU OR 74/2008).

Karl, M., Gross, A., Leck, C. and Pirjola, L. (2010) New particle formation in the High Arctic: Observations and model simulations. *Geophys. Res. Abstr., 12,* EGU2010-8393.

Köhler, H. (1936) The nucleus in and the growth of hygroscopic droplets. *Trans. Far. Soc.*, *32,* 1152-1161.

Kunkel, B.A. (1971) Fog drop-size distributions measured with a laser hologram camera. *J. Appl. Meteorol.*, *10,* 482-486.

Kunkel, B.A. (1982) Microphysical properties of fog at OTIS FAB. Hanscomb Mass., Air Force Geophys. Laboratory (Research Report, 767) (AFGL-TR-82-0026) pp. 11–15.

Langmuir, I. and Langmuir, D.B. (1927) The effect of monomolecular films on evaporation of ether solutions. *J. Phys. Chem.*, *31,* 1719-1731.

Li, Z., Williams, A.L., and Rood, M.J. (1998) Influence of soluble surfactant properties on the activation of aerosol particles containing inorganic solute. *J. Atmos. Sci.*, *55,* 1859–1866.

Mason, B. J. (1971) The Physics of Clouds. Clarendon press, Oxford, 671 pp.

McDonald, J.E. (1963) Rain washout of partially wettable insoluble particles. *J. Geophys. Res.*, *68,* 4993-5003.

McFiggans, G., Artaxo, P., Baltensberger, U., Coe, H., Facchini, M.C. , Feingold, G., Fuzzi, S., Gysel, M., Laaksonen, A., Lohmann, U., Mentel, T.F., Murphy, D.M., O'Dowd, C.D., Snider, J.R. and Weingartner, E. (2006) The effect of physical and chemical aerosol properties on warm cloud droplet activation. *Atmos. Chem. Phys.*, *6,* 2593-2646.

McNeill, V. F., Schwier, A. N., Li, Z., Svokos, E. R., Mitroo, D. and Seltzer, J. (2010) Surface-Bulk partitioning of organic material in aqueous aerosols. *Geophys. Res. Abstr.*, *12,* EGU2010-1630.

Okuda, T., Tomine, K. and Sugawara, H. (2009) Direct photographic method for measuring droplet size distribution in fog. *SOLA*, *5,* doi:10.2151/sola.2009-004, 13-16.

Pandis, S.N., Seinfeld, J.H. and Pilinis, C. (1990) Chemical composition differences in fog and cloud droplets of different sizes. *Atmos. Environ., 24A,* 1957-1969.

Pruppacher, H.R. and Klett, J.D. (1997) Microphysics of clouds and precipitation. 2nd ed. Boston, Kluwer Pub. Inc.

Nenes, A., Charlson, R.J., Facchini, M.C., Kulmala, M., Laaksonen, A. and Seinfeld, J.H. (2002) Can chemical effects on cloud droplet number rival the first indirect effect? *Geophys. Res. Lett.*, *29,* 1848, doi:10.1029/2002GL015295.

Roedel, W. (1992) Physik unserer Umwelt: die Atmosphäre. Berlin/Heidelberg, Springer-Verlag. pp. 162-169.

Rogers, R. R. and Yau, M. K. (1989) A short course in cloud physics. 3rd ed. Oxford, Pergamon Press (International Series in natural philosophy, 113).

Shulman, M.L., Jacobson, M.C., Charlson, R.J., Synovec, R.E. and Young, T.E. (1996) Dissolution behavior and surface tension effects of organics in nucleating cloud droplets. *Geophys. Res. Lett.*, *23,* 277-280.

Sorjamaa, R., Svenningsson, B., Raatikainen, T., Henning, S., Bilde, M. and Laaksonen, A. (2004) The role of surfactants in Köhler theory reconsidered. *Atmos. Chem. Phys.*, *4,* 2107-2117.

Taylor, F. W. (2005) Elementary climate physics. Oxford, Oxford University Press. p. 65.

Tuckermann, R. and Cammenga, H.K. (2004) The surface tension of aqueous solutions of some atmospheric water-soluble organic compounds. *Atmos. Environ.*, *38,* 6135-6138.

Vázquez, G., Alvarez, E., Navaza, J. M., Rendo, R. and Romero, E. (1997) Surface tension of binary mixtures of water + monoethanolamine and water + 2-amino-2methyl-1-propanol and tertiary mixtures of these amines with water from 25°C to 50°C. *J. Chem. Eng. Data, 42,* 57-59.

Appendix A

Average results obtained in the experiments performed with NaCl and MEA solution at different concentrations.

48

Conc.: concentration; Mag: Magnification; n: number of digital images analysed; Major: diameter from the best fit ellipse. Ci: Circularity. Feret: diameter. s.d.: standard deviation. n/a: not available.

# Run	Solution	Conc. (%)	Exposure (min)	Mag	n	#	Average Size (µm2)	Area Fraction (%)	Major (µm)	Ci (0-1)	Feret (µm)
TA8	NaCl	0,6	30	x10	5	2437	44,0	7,0	9,4	0,8	10,4
					s.d.	817	5,1	2,6	0,5	0,0	0,5
TA8	NaCl	0,6	30	x20	5	570	42,2	6,2	9,0	0,7	9,8
					s.d.	81	3,4	1,3	0,0	0,0	0,4
TA9	NaCl	0,6	30	x10	5	974	31,8	1,9	8,0	0,8	9,0
					s.d.	618	0,9	1,3	0,0	0,0	0,0
TA9	NaCl	0,6	30	x20	5	346	31,2	2,9	8,0	0,7	8,4
					s.d.	145	1,8	1,4	0,0	0,0	0,5
TA2	NaCl	2,6	30	x10	5	24	295,5	0,4	20,8	0,7	23,0
					s.d.	7	68,7	0,1	1,9	0,0	2,3
TA2	NaCl	2,6	30	x20	1	615	30,4	4,9	8,0	0,7	8,0
TA3	NaCl	2,6	30	x10	3	42	262,5	0,7	20,3	0,6	23,0
					s.d.	15	63,3	0,2	2,5	0,0	2,0
TA3	NaCl	2,6	30	x20	5	340	30,9	2,8	7,8	0,7	8,6
					s.d.	143	2,8	1,4	0,4	0,0	0,5
TA4	NaCl	2,6	30	x10	5	2010	39,7	5,1	8,4	0,8	9,4
					s.d.	504	4,6	1,8	0,5	0,0	0,5
TA4	NaCl	2,6	30	x20	5	643	41,5	7,0	8,6	0,7	9,4
					s.d.	126	5,2	1,6	0,5	0,0	0,5
TA5	NaCl	5,3	30	x10	5	1173	36,2	2,6	8,2	0,8	9,0
					s.d.	810	2,4	1,9	0,4	0,0	0,0
TA5	NaCl	5,3	30	x20	5	321	29,9	2,5	7,8	0,7	8,2
					s.d.	118	1,4	1,0	0,4	0,0	0,4
TA6	NaCl	5,3	30	x10	2	1027	41,0	2,6	9,0	0,7	10,0
					s.d.	132	0,7	0,3	0,0	0,0	0,0
TA6	NaCl	5,3	30	x20	5	216	38,4	2,2	8,6	0,7	9,4
					s.d.	54	3,4	0,7	0,5	0,0	0,5
TA7	NaCl	5,3	30	x10	5	1279	36,8	2,5	8,4	0,7	9,4
					s.d.	410	3,7	0,6	0,5	0,0	0,5
TA7	NaCl	5,3	30	x20	4	322	35,1	2,9	8,3	0,7	9,0
					s.d.	84	2,9	1,0	0,5	0,0	0,0
TA10	MEA	0,6	30	x10	2	505	29,6	1,0	8,0	0,8	8,5
					s.d.	77	2,7	0,2	0,0	0,0	0,7
TA10	MEA	0,6	30	x20		n/a	n/a	n/a	n/a	n/a	n/a
TA11	MEA	0,6	30	x10	10	239	168,7	0,6	14,5	0,7	16,3
					s.d.	352	156,6	0,6	7,2	0,0	8,2
TA11	MEA	0,6	30	x20	9	115	76,6	0,9	10,2	0,6	11,2
					s.d.	120	100,1	0,9	4,9	0,1	5,3
TA12	MEA	2,6	30	x10	1	1036	46,3	3,1	9,0	0,7	10,0
TA12	MEA	2,6	30	x20		n/a	n/a	n/a	n/a	n/a	n/a
TA13	MEA	2,6	30	x10	1	327	48,5	1,0	9,0	0,6	10,0
TA13	MEA	2,6	30	x20	6	274	109,4	2,2	10,5	0,7	11,7
					s.d.	194	196,3	1,5	8,1	0,0	9,0
TA14	MEA	5,3	30	x10		n/a	n/a	n/a	n/a	n/a	n/a
TA14	MEA	5,3	30	x20		n/a	n/a	n/a	n/a	n/a	n/a
TA15	MEA	5,3	30	x10		n/a	n/a	n/a	n/a	n/a	n/a
TA15	MEA	5,3	30	x20		n/a	n/a	n/a	n/a	n/a	n/a
TA16	MEA	5,3	15	x10		n/a	n/a	n/a	n/a	n/a	n/a
TA16	MEA	5,3	15	x20		n/a	n/a	n/a	n/a	n/a	n/a

50

REPORT SERIES	REPORT NO. OR 58/2010	ISBN: 978-82-425-2274-0 (print) 978-82-425-2275-7 (electronic)
SCIENTIFIC REPORT		ISSN: 0807-7207
		ISSN: 0807-7185

DATE	SIGN.	NO. OF PAGES	PRICE
1.10.2010		49	NOK 150.-

TITLE	PROJECT LEADER
Test of the NILU fog chamber as experiment reactor for droplet growth	Matthias Karl
	NILU PROJECT NO. E-109103

AUTHOR(S)	CLASSIFICATION *
Matthias Karl and Susana López-Aparicio	A
	CONTRACT REF.

REPORT PREPARED FOR
NILU

ABSTRACT

This report covers part of the work performed as part of the project Fog-TEST. A new fog-chamber was designed and characterized in the project to cover the needs for performing the experiments. The current fog-chamber, which modification has been based on the experiments performed and the improvement of its functionality, consists basically of the chamber as container, a humidifier and a constant output atomizer. In addition, droplet sampler was modified and adjusted in the framework of the project. In order to analyse the droplet size, a methodology was developed to study droplets impact prints on coated slides by microscopy and subsequent processing and quantification.

NORWEGIAN TITLE

"Test av NILU tåkekammer som eksperimentreaktor for dråpevekst"

KEYWORDS		
Fog-chamber	Droplet growth	Amines

ABSTRACT (in Norwegian)
Denne rapporten beskriver deler av arbeidet utført i prosjektet Fog-TEST. Et nytt nedbørkammer ble satt opp og karakterisert i prosjektet for å utføre eksperimentene. Funksjonalitet av eksisterende nedbørkammer ble stadig forbedret basert på utførte eksperimenter. Nedbørkammeret består i utgangspunktet av en 1.5 m^3 stor beholder utrustet med en luftfukter og en generator (atomizer) som leverer partikler (og dråper) med konstant produksjonsrate. I tillegg ble en kommersiell prøvetaker endret og justert innenfor rammen av prosjektet. For å analysere dråpestørrelse, ble en metodikk utviklet basert på mikroskopiske lysbilder av dråpens avtrykk i prøvene fra den nye dråpetaker, og deretter behandlet og kvantifisert.

* Classification   *A*   *Unclassified (can be ordered from NILU)*
                       B   *Restricted distribution*
                       C   *Classified (not to be distributed)*

NILU is an independent, nonprofit institution established in 1969. Through its research NILU increases the understanding of climate change, of the composition of the atmosphere, of air quality and of hazardous substances. Based on its research, NILU markets integrated services and products within analyzing, monitoring and consulting. NILU is concerned with increasing public awareness about climate change and environmental pollution.

NILU Norsk institutt for luftforskning
Norwegian Institute for Air Research